The Effect of Bathymetry Changes on Meridional Overturning Currents

Marte Voorneveld
5911591

June 8, 2020

Abstract

We investigate the effect of changing geometries in a simple ocean general circulation model. Using highly idealized forcings we compare the the situations for every 5 Milion year (Ma) time step from 65Ma to the present day situation. The present day simulation was used as a control. The model result shows a reversal of the flow through the panama gateway in the early Miocene coinciding with the closure of the Thetys seaway. We also observe a system that is extemely senstive to the position of the Indian Continent in the Paleocene. Furthermore we observe large differences in the thermohaline circulations in comparison to the present day situation.

The abstract still needs some work as my conclusions are still so weak. Formatting the document is also not finalized. Some half empty pages are still present. But dealing with formatting is not efficient when the paper is not in its final state.

1 Introduction

The geography and bathymetry (depth profile of the ocean) of our planet is an ever-changing phenomenon. In the last 120 Ma (million years), the earth moved from having one major oceanic system in the Pacific with a single large continent to the current 3 ocean system (Besse and Courtillot 2002). The Bathymetry changes that occurred in this period are characterized by the opening and closing of certain passages through which exchange of water between the oceanic basins is observed. These passage changes are a vital part of understanding the global thermohaline circulation. The exact timing of passage openings is a topic of rigorous debate in literature (Scher and Martin 2006, Schmidt 2007).

One of the changes on which there is a consensus is the inception and expansion of the Atlantic ocean. This expansion results in a decrease in the size of the Pacific basin. The creation of the Atlantic basin has had major effects on the earth's climate, especially resulting in massive localized changes such as the temperate European climate. The North Atlantic meridional overturning circulation (AMOC) is now understood to be essential in the present-day thermohaline circulation. The AMOC is the result of a deep water formation in the North Atlantic. In the northern Atlantic, there is a northward flow of water with substantial heat energy. This water sinks when it reaches the arctic waters. This is because the flow rapidly loses its heat energy due to the large temperature gradient in the arctic. The loss of energy causes an increase in density and subsequent sinking of the flow. This flow is often called the " ocean Conveyer belt", a term first coined by Broecker 1991. However, it is unknown when exactly this northern sinking started. With the past nonexistence of the Antarctic Circumpolar Current (ACC) and the relatively small size of the Atlantic ocean, the AMOC must have seen its inception sometime in the last 40Ma (Abelson and Erez 2017).

The result of these bathymetry changes on the oceanic stream function and the resulting overturning currents is something that has been previously studied by Mulder et al. 2017. They however found that using a 3D model for different geographies in each of the model years fails to simulate the onset of the Northern sinking AMOC that is physically observed. They use a continuation method for the forcing of each timestep, taking the previous timestep as a reference. Here we propose to use a similar general ocean circulation model (GCM) with only a changing bathymetry and highly simplified zonal forcings. To accomplish this we use the relatively young GCM Veros.

This paper will focus on the effect of changes in bathymetry when using highly simplified zonally averaged forcings for the last 65Ma. The results of the model will be used to estimate global changes in oceanic throughflow at oceanic passages. Furthermore, the strength of the meridional overturning currents (MOC) and the thermohaline circulation will be studied.

2 Methods

2.1 Veros

Veros is an ocean general circulation model (GCM) based on the successful PyOm2 model (Hafner et al. 2018). It was designed from the ground up with flexibility in mind. This flexibility cuts valuable time spent on figuring out the often cumbersome Fortran models of the past. Veros is specifically well suited for researching the effect of changes in both forcings and bathymetries. They can be easily edited using Python. These features in particular are heavily used in this paper. One of the most extensively used attributes is the fact that any bathymetry can, without further manual specifications, be used for stream function calculation. The fact that Veros is fully written in Python is also useful as it is a far more widespread language than Fortran and it is thus much easier to teach Veros to new students.

In this case, the models used in this paper are run on an 8 core (16 threads) machine using an MPI CPU configuration of 1 node. This is sufficient for the lower resolution models used in this paper. But it is noted that Veros does allow the usage of multiple nodes to do calculations on much higher resolution problems.

2.2 Model Setup

2.2.1 Model Domain

The domain of the model is bounded by longitudes $\phi_E = -180°$ and $\phi_W = -180°$ and latitudes $\theta_N = 80°$ and $\theta_S = -80°$ with periodic boundary conditions in the zonal direction. The depth profile has 15 layers with grid stretching (fig. 1). The grid stretching relation is such that surface layers are much shallower than deep water layers. There are 90×40 horizontal grid points to make a $4° \times 4°$ resolution model.

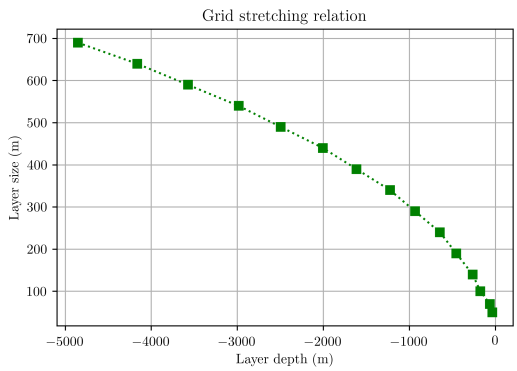

Figure 1: Figure of the grid stretching relation used.

2.2.2 Surface Forcings

The model used, uses restoring boundary conditions. Restoring the boundary at the surface of the oceanic basin to be a value based on a forcing field for Sea Surface Temperature (SST), Sea Surface Salinity (SSS), wind stresses (τ) and heat flux. Choosing the correct forcing for the ocean is very important. It is known that in general circulation models the MOC is highly sensitive to even small changes in surface forcings (Milliff et al. 1999). Attempts at making these forcings highly idealized have often been made in the past with varying rates of success(Bryan 1987; Mulder et al. 2017). We note the fact that using idealized forcings will probably induce the errors, especially in the shape of the thermohaline circulations. The use of idealized forcings is however justified here because we are only interested in large scale features of the AMOC and the wind-driven circulations.

Several methods are explored when it comes to creating these idealized forcings. In the Mulder et al. 2017 paper an analytic forcing profile was used for wind stress, SST, and SSS (fig. 2). Veros is however a seasonally forced model. Using these simplified forcings would thus fail to capture seasonal changes especially in the SST. There have been studies suggesting that these seasonal forcings can have large effects on the strength of the meridional overturning circulation (Schmittner and Stocker 2001). Here we propose to take the SSS and SST profiles as zonal means of realistic forcings. We use $1^\circ \times 1^\circ$ forcings from the ECMWF public dataset a basis (ECMWF 2020). While the zonal wind stress is set to the simple profile proposed by Bryan 1987. The choice of this analytic profile was made over a zonally averaged forcing mirrored along the equator ($\mu(\tau_x)$). These were both tested on the present-day configuration to see which of these forcings most accurately captures the present-day MOC. After some initial tests, we found that $\mu(\tau_x)$ is very weak in the sub polar regions and subsequently fails to force the North Atlantic Deep Water formations (NADW).

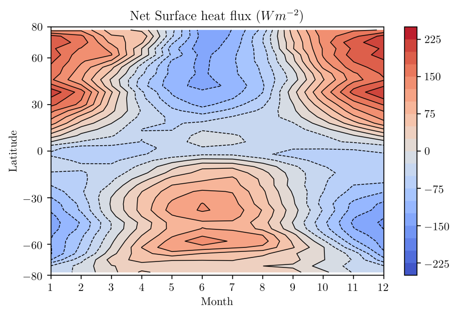

(a) Net Heat flux

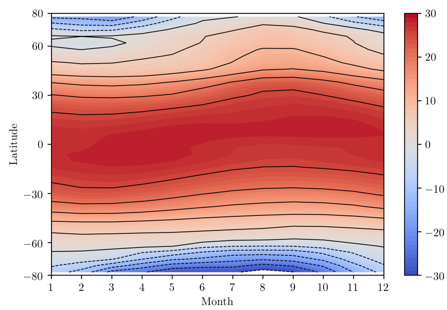

(b) SST profile

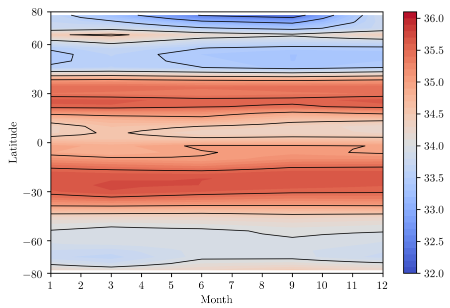

(c) SSS profile

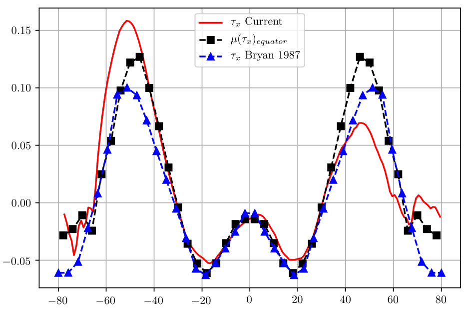

(d) τ_x profile

Figure 2: Idealized forcing profiles for **a)** The net heat flux, **b)** The Sea surface Temperature

2.2.3 Forcing bias

The forcings we use here have large errors compared to reality. This can be seen if we compare the original realistic forcings to the zonal mean of these forcings. In fig. 3 the errors compared to present-day forcings are shown. there is a particularly large discrepancy in the Atlantic, which has a much higher salinity in reality than in our forcing. This may have implications on the thermohaline circulation we will observe in our model. It is furthermore noted that the northern Atlantic ocean is much warmer in reality than in our model, which again possibly can affect the thermohaline circulation. We also note that the temperature on earth was also much higher in the early part of the 65Ma period (Hansen et al. 2013). We neglect this effect because we use the same forcing for each time step. Therefore, it is not possible to compare our results directly with existing proxies. However, studying the effect of geography changes specifically is much clearer using this method.

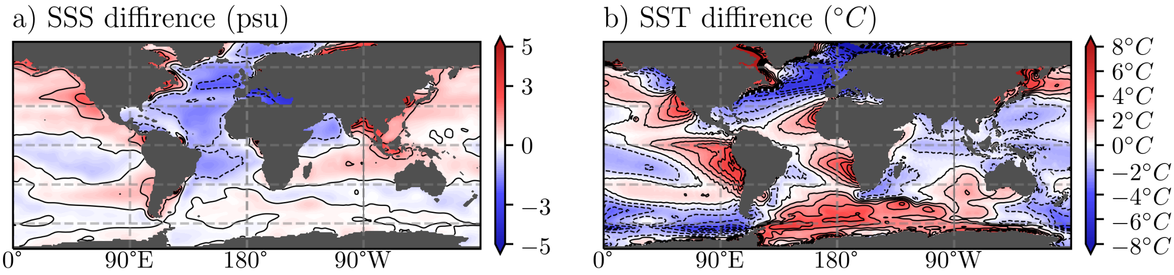

Figure 3: Figure showing errors in surface forcing. As a diffirence between ECMWF forcings and zonal mean forcings. As a monthly average. Here positive values are over estimations of realistic forcings. Errors for: **a)** the SSS difference with contours every 1 psu and **b)** the SST difference with contours every 1 $^\circ C$

2.2.4 Initial conditions

The model is started with an initial temperature and salinity profile that is, like the forcings taken from observational data (ECMWF 2020). The temperature profiles again use zonal means. This results in the profile seen for the situation around the equator in fig. 4.

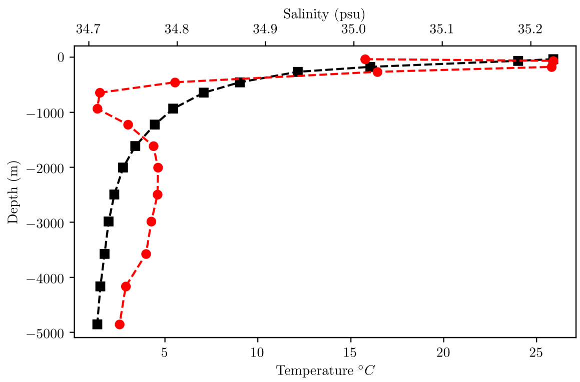

Figure 4: Figure showing the temperature and salinity profiles at $2^\circ N$. Black squares indicate the Temperature profile and red circles indicate the salinity profile.

2.2.5 MOC stream function

The global Meridional Overturning Circulation Ψ_{MOC} is defined as the zonally integrated meridional volume transport of water in the worlds oceans. It can be written down as:

$$\Psi_{MOC}(y,z) = \int_z^0 \int_{-180^\circ}^{180^\circ} v(x,y,z')dxdz'.$$

Here v is the meridional component of the velocity. Ψ_{MOC} is thus a stream function of the zonally integrated volume transport in the Earth's ocean basins. Plotting this stream function can give a lot of insight into the deep water transport associated with the thermohaline circulation. In this paper, we hope to capture these deepwater transport formations. In particular, we are looking for the shape of the North Atlantic deep water (NADW) and the Antarctic Bottom Water (AABW) formations.

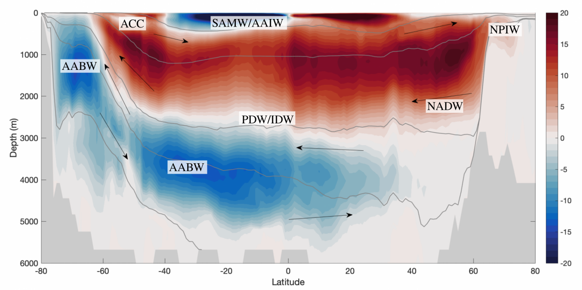

Figure 5: Meridional overturning circulation with schematic arrows indicating flow direction. Also including general areas of flow. AABW: Antarctic Bottom Water, NADW: North Atlantic Deep Water, NPIW: North Pacific Intermediate Water, PWD: Pacific Deep Water, IDW: Indian Deep Water, SAMW: Subantarctic Mode Water, AAIW: Antarctic intermediate Water, ACC Antarctic Cicumpolar Current. MOC taken from Forget et al. 2015.

2.2.6 Barotropic Stream Function

It is furthermore interesting to look at an expression for the transport of ocean gyres. We know that the depth-integrated flow must be horizontally non-divergent. Thus a stream function Ψ_b can be introduced. Where $v(x, y, z)$ is the meridional velocity:

$$U = -\frac{\partial \Psi_b}{\partial y}; V = \frac{\partial \Psi_b}{\partial x} \tag{1}$$

$$\Psi_b = \int_{easternbdy}^{x} \int_{-D}^{0} v(x', y, z) dz dx' \tag{2}$$

This so-called barotropic stream function Ψ_b is defined by integrating the meridional transport westward from the eastern boundary of the domain. It is a useful tool to look at the shape and gyres associated with the major ocean current systems. By using the Sverdrup relation

$$\int_{-D}^{0} v(x, y, z) dz = \frac{1}{\beta \rho_{ref}} \vec{\hat{z}} \cdot \nabla \times \tau$$

first proposed by Sverdrup 1947 we can look at a schematic diagram of the barotropic stream function based on the prevailing zonal winds. fig. 6 shows a schematic of this relation. It is easily visible how the prevailing zonal winds relate to the wind stress forcing seen in fig. 2. The calculation of the barotropic stream function without easily defined boundaries is quite a bit more cumbersome than a simple integration from the eastern boundary. Veros uses a process in which special treatment is given to boundaries with island integrals.

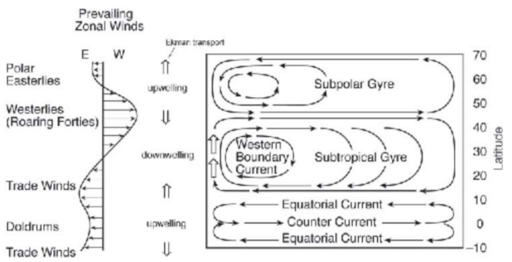

Figure 6: Schematic of the barotropic stream function based on the Sverdrup relation. Showing the subpolar and subtropical Gyres and equatorial currents. Figure taken from John Marshall 2012

2.2.7 Passage throughflow

For each of the passages mentioned in section 2.3 it is interesting to talk about the total volume transport through each of the passages discussed. This is done using a simple integration to calculate the volumetric flux through each passage. The volumetric flux is defined as

$$Q = \iint_A \vec{u} \cdot d\vec{A} \tag{3}$$

Where we integrate the zonal velocity over an area A in the latitude-vertical direction that is normal to this velocity. For each passage a suitable location is chosen such that there are no boundaries next to the passageways, this is done for each time step. Then the u component of the flow is used to compute the total flow. This method is the same for each of the passages and thus we can study the effect of changes in bathymetry to on the relative strength of the flow. However, it should be noted that these values may not represent real physical values. As the passages in a 4° model are often only a few grid cells wide. Resulting in discrepancies in the calculation of the throughflow due to boundary conditions. In fig. 7 An overview is shown of all the passages discussed in this paper. There may be a more accurate way to calculate the throughflows. The alternative method uses the output of the Barotropic stream function discussed in Section 2.2.6. This also gives us a measure of throughflow in each grid cell. It is however difficult to get accurate values from this in Veros because the current version does not display the boundary values for the stream function.

There is also an overview of the naming scheme used for each of the continents and oceans in our discussion.

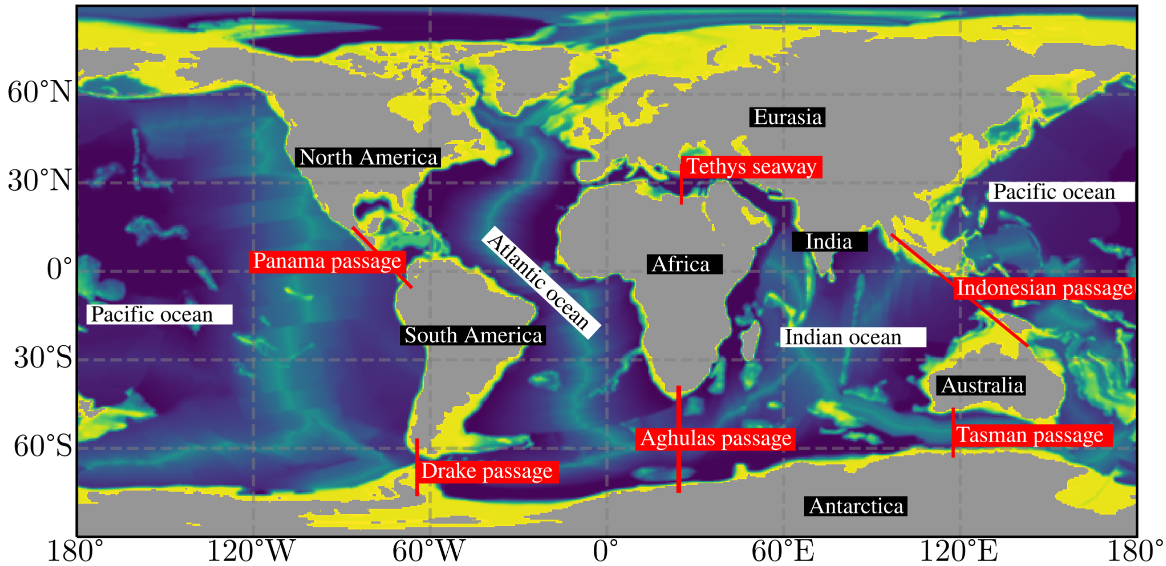

Figure 7: Schematic image showing the 30 Ma bathymetry in $0.5° \times 0.5°$. Overlayed in red are the passages we study. In black the continents and in white the oceanic basins.

2.3 Creating Bathymetries

To facilitate the model a set of 14 bathymetries was created in 5Ma time steps. These run from 65Ma to the present-day configuration. These were reconstructed from bathymetries gained in Baatsen et al. 2016. These bathymetries which originally were $0.5° \times 0.5°$ have been scaled to a $4° \times 4°$ model using Gaussian interpolation. Next, the land masks were manually edited to include passages and exclude some inland seas. Due to the low resolution of the model, choices have to be made concerning the opening of certain passages. One of the choices that were made is that the northern Arctic sea is closed off in all of the bathymetries. This is mainly since $4° \times 4°$ models do not have enough resolution to facilitate this sea and Veros lacking the ability to have polar flow. The main events that shape the oceanic passages can be divided into periods. These periods are defined in table 1.

	From	Until
Paleocene	65Ma	55Ma
Eocene	50Ma	35Ma
Oligocene	30Ma	25Ma
Miocene	20Ma	10Ma
Pliocene	5Ma	present

Table 1: Time periods covered by this paper

The discussion on each time period is split. Here we address each of the periods and their respective changes.

2.3.1 Paleocene

In the Paleocene a vast Pacific exists almost serving as a single basin. This period is largely characterized by the growth and development of a larger atlantic basin. Subsequently a decrease in size of the pacific basin is also observed. The drake passage is explicitly chosen to be closed in this time period, there is some evidence of it being opened in the paleocene due to a major change in the motion of the South American and Antarctic plates until about 50Ma (Livermore et al. 2005). However, the evidence proposes a shallow opening of less than 1 km in depth. These uncertainties and the shallow nature of the opening has led to the decision to close the passage until its certain deep water connection starting after the late Eocene as also indicated by Livermore et al. 2005.

It is also of interest to note the existence of a range of islands between the Indian continent and the Eurasian continent which dissapears in this period. These islands are called the Kohistan-Ladakh Arc (Jagoutz, Bouilhol, and Upadhyay 2009). These may have had quite significant effect on the flow through the thetys seaway and are thus an interesting topic to discuss later on.

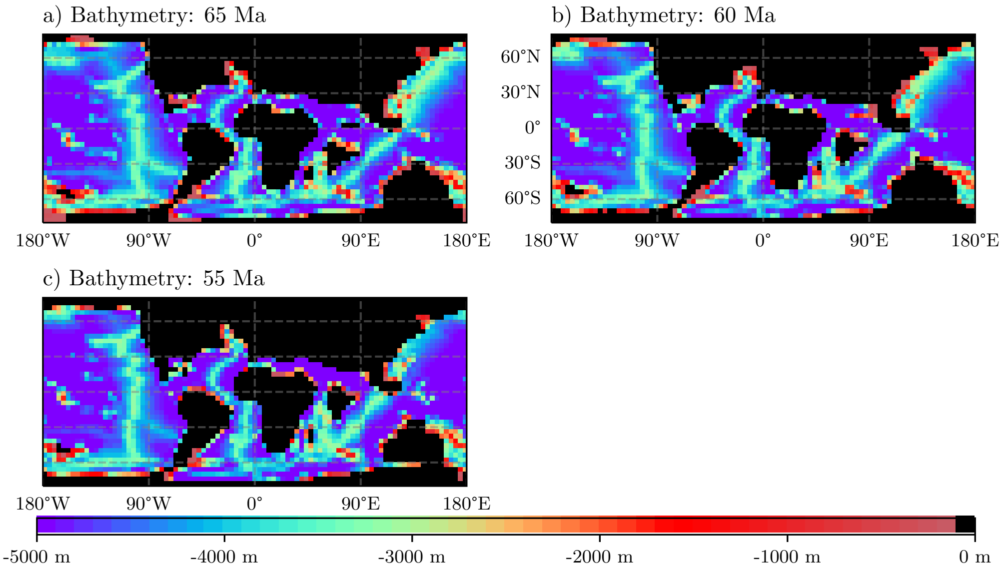

Figure 8: Paleocene Bathymetries showing **(a)** The bathymetry of 65 Ma. **(b)** The bathymetry of 60 Ma. **(c)** The bathymetry of 55 Ma

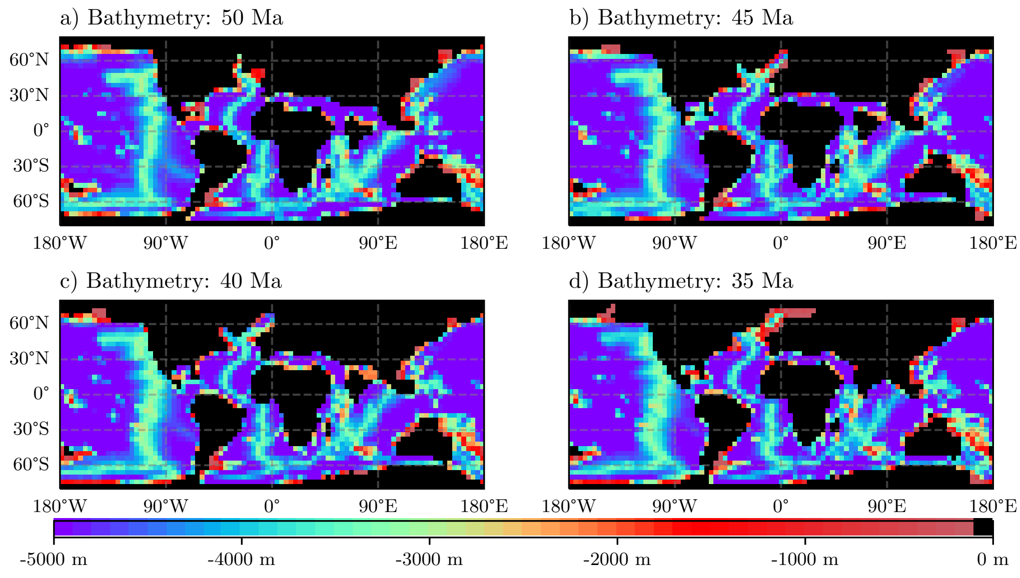

Figure 9: Eocene Bathymetries showing **(a)** The bathymetry of 50 Ma. **(b)** The bathymetry of 45 Ma. **(c)** The bathymetry of 40 Ma.**(d)** The bathymetry of 35 Ma

2.3.2 Eocene

The Eocene in contrast to the Paleocene is distinguished by the opening of certain passages connecting oceanic basins. These effects are often studied extensively for each individual passage in literature. Choosing the exact timing for opening the passages is done manually by looking at often active research. The first of such passages to open is the Tasman passage which is opened at 35Ma as a shallow passage slowly growing in size(Lawver and Gahagan 2003). The Tasman passage opening is believed to have had a large impact on the onset of the Atlantic circumpolar current (ACC). Some authors even suggests its influence on the onset of a early "proto-ACC" (Sarkar et al. 2019). This proto-ACC may have caused upwelling of northern-sourced nutrient-rich deep equatorial Pacific waters in the south Pacific. However, this is assuming an open drake passage, which does not exist in our bathymetries. Thus, this upwelling will likely not be observed until the early Oligocene.

From the onset of the early Eogene the Indian Continent has been fast moving towards the north slowly closing the northern passage between the Indian ocean and the Tethys seaway. The deep water passage is closed from 35Ma based onwards Najman et al. 2010. This limits the throughflow through the Thetys seaway to purely east of the Indian continent. Which is now in effect part of the larger Eurasian continent.

2.3.3 Oligocene

From the onset of the Oligocene The Total circulation of water around the Antarctic basin is finalized by the opening of the shallow Drake passage at around 30Ma. 30Ma is specifically chosen to differentiate between the opening of the drake and Tasman passages. Especially since there is still some debate on the exact timing of drake passage opening (Scher and Martin 2006; Livermore et al. 2005). These openings coincide with the onset of the ACC that has had major effects on the global climate variability. Furthermore, The Oligocene is characterized by the further expansion of the Atlantic basin and a shallower Thetys seaway. Furthermore a deep water area starts existing between what is now Greenland and the European continent. This water basin is now known to be central to the deep water formations of the northern Atlantic.

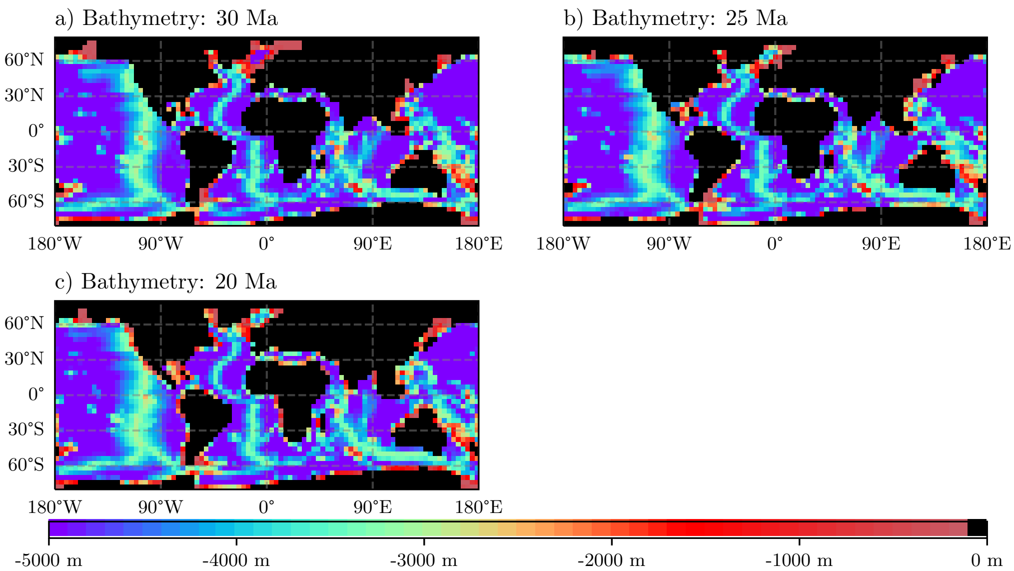

Figure 10: Oligocene bathymetries showing: **(a)** The bathymetry of 30 Ma. **(b)** The bathymetry of 25 Ma. **(c)** The bathymetry of 20 Ma.

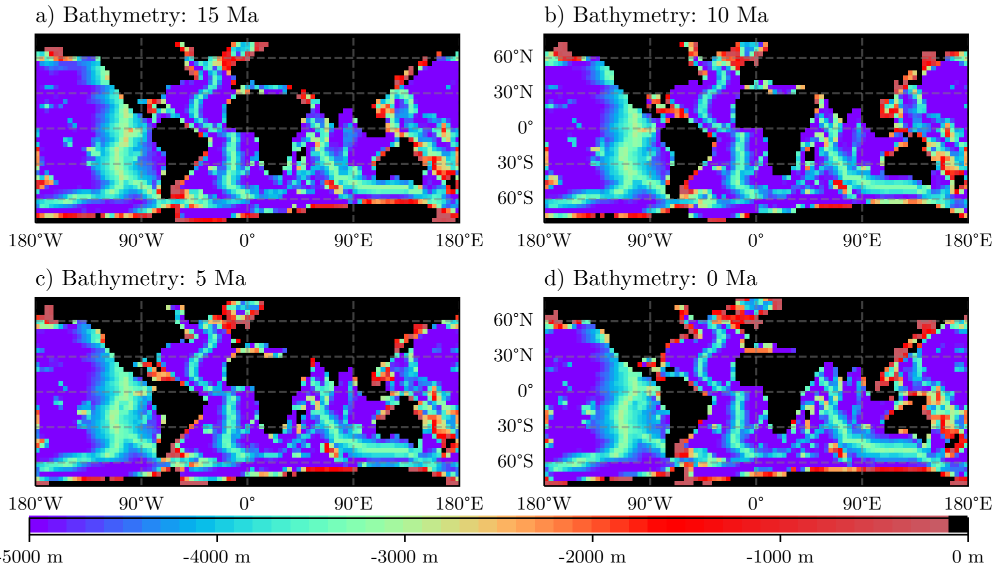

Figure 11: Miocene bathymetries showing **(a)** The bathymetry of 15 Ma. **(b)** The bathymetry of 10 Ma. **(c)** The bathymetry of 5 Ma.**(d)** The present day bathymetry

2.3.4 Miocene

Finaly, the Miocene is Characterized by Some more passage closures. The Tethys seaway had been decreasing in size for the duration of our bathymetries. It finally fully detaches the mediteranian sea from the Indian ocean from 15Ma onward(Hamon et al. 2013). Then another major change occurs with the closure of the panama seaway from 5Ma onward (Molnar 2008; Pindell et al. 1988). Stopping the mid latitude throughflow between the Atlantic and Pacific basins. The throughflow in the panama seaway is believed is believed to have reversed in direction with the onset of the decrease in size and subsequent closure of the Thetys ocean (von der Heydt and Dijkstra 2006; Omta and Dijkstra 2003). Something that will be studied more closely in the discussion of our results.

2.3.5 Pliocene

3 Results

3.1 Model runs

The model was run for 500 years for each of the 14 time steps. Accounting for a total of 7000 years of model time. The timings are shown in table 2. We see that the total integration time is quite long but in general manageable. We note that it would be possible to significantly speed up our work by using many nodes in parallel instead of a single node in succession.

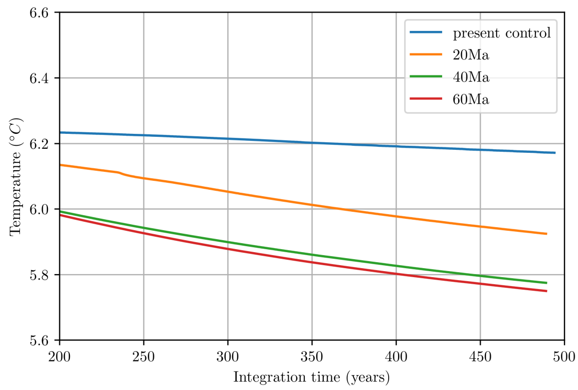

Figure 12: Total globally averaged temperature ($^{\circ}C$) for presentday (blue), 20Ma (orange), 40Ma (green) and 60Ma (red). From 200 to 500 years integration.

Year	$\Delta time$	$time$	ΔT	ΔS
present day	1'01"	8:30	-2.1978	-1.8629
5Ma	1'01"	8:30	-2.8292	-2.5038
10Ma	1'01"	8:30	-2.7764	-1.8219
15Ma	1'02"	8:40	-6.1497	-2.6299
20Ma	1'01"	8:30	-5.3202	-1.9109
25Ma	1'02"	8:40	-5.3201	-1.9341
30Ma	1'03"	8:30	-3.0994	-1.5755
35Ma	1'00"	8:30	-0.3163	-1.6289
40Ma	1'02"	8:40	-5.1253	-1.7728
45Ma	1'00"	8:20	-5.1196	-1.7066
50Ma	1'00"	8:20	-4.9925	-1.6592
55Ma	1'01"	8:30	-4.9158	-1.6586
60Ma	1'02"	8:40	-5.5853	-1.6902
65Ma	1'03"	8:50	-6.3302	-1.8980

Table 2: $\Delta time$ is the time per integration in minutes'seconds". $time$ is the time in hours for each run. ΔT is the average temperature gradient for the last 10 time steps in $10^{-4}C$ per year. ΔS is the average salinity gradient for the last 10 time steps in $10^{-4}psu$ per year.

3.2 Control setup

To get an understanding of the quality of the model and thus if any of the results resemble reality, one can compare the present day setup of the model to an existing model with realistic forcings. Also, the model can be compared to another similar higher resolution model. This can be a useful tool to see what aspects of the present day situation are captured by the model and more importantly which nuances are lost. General circulation models with a resolution comparable to the model used in this paper often loose major features having to do with the overturning circulation (Stone and Risbey 1990). Especially the restoring boundary conditions at the surface are troublesome where capturing artifacts of the thermohaline circulation is highly dependant on surface salinity and temperature profiles. This dependance is even further complicated by the highly idealized forcings used here (section 2.2.3). To get a qualitative look at the error introduced in our model, the BSF and the MOC outputs are studied together with their temperature profiles. We compare our control setup with a Veros run with realistic forcings on the same setup.

3.2.1 BSF control

Too look at the quality of the barotropic stream function we compare the barotropic stream function of our model to the Veros model with realistic forcings. This model was made with the standard Veros setup with custom open Indonesian passage. In fig. 13 we see the barotropic stream function compared. Here we see quite a few differences. Notably, the strength of the gyres is much weaker in our simplified forcings case. This can mostly be explained by the generally weaker wind stresses in these regions. Also, in our simplified model there is a notable absence of the sub polar gyre in the northern Atlantic. The difference in strength of the subtropical gyres is about $10Sv$ on average. Reaching a $20Sv$ difference in the subtropical gyre in the Indian ocean.

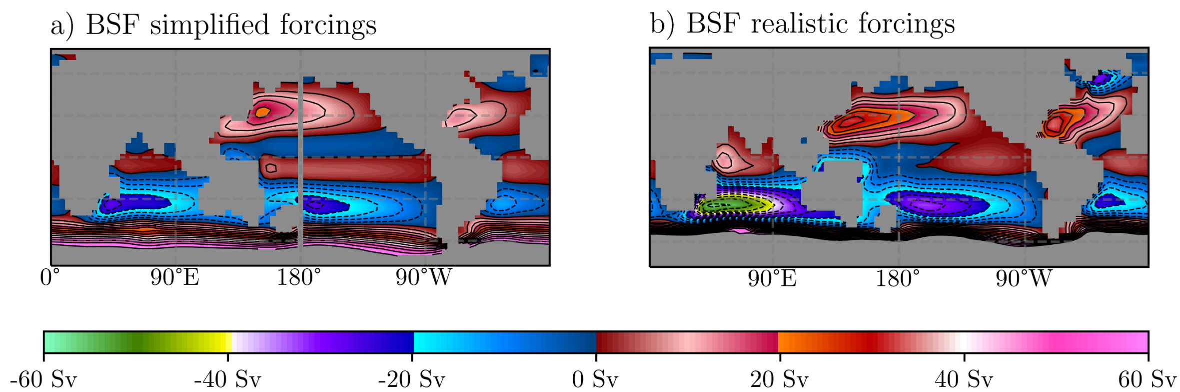

Figure 13: Barotropic stream function with contours every 5 Sv. For **a)** simplified forcings and **b)** realistic forcings.

3.2.2 Quality of the MOC

Next we look at the MOC stream functions and compare them between the two models. Here we must note the difference in geometry between the two models. This is due to the fact that we use an interpolated version in the simplified forcings case. That is different from the geometry used by Veros. In fig. 14 we see the MOC stream function for the simplified and realistic models. Here the real problem of using simplified forcings is visible. The overturning circulation with the simplified forcings is extremely weak compared to the overturning circulation with simplified forcings. We note that several key features are not captured by both models. The first, most striking is the complete absence of the AABW cell. This feature seems to not be captured at all in the model. This might be because of the extremely simplified method of simulating sea ice in the model. Sea ice extend in the arctic is known to be central to the formation of the AABW (Hansen et al. 2016). The NADW formation is captured both models. It is however much weaker in the case of simplified forcings. The main diffirence being the strength of the IDW/PDW cell. Which is only 4 Sv in the simplified model. While the realistic forcing model does a better job at around 15Sv. We note the weaker overturning as being a generic feature of our model in the chapter discussing the overturning circulation for each time step.

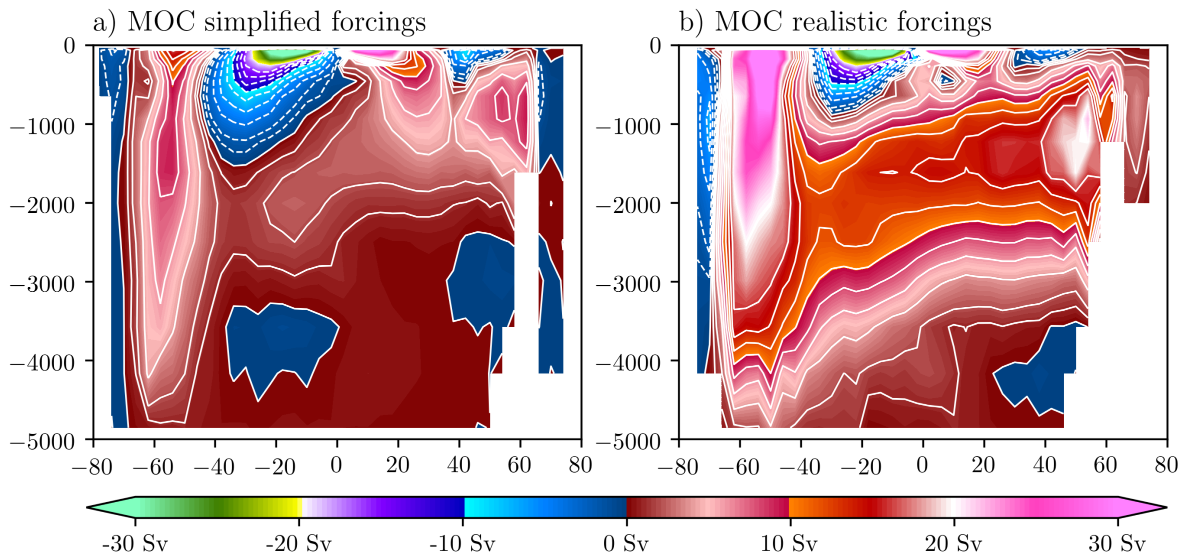

Figure 14: MOC stream function with contours every 2 Sv. For **a)** simplified forcings and **b)** realistic forcings. Negative values (dashed lines) indicate counterclockwise circulation

3.3 Passage throughflow

As discussed in section 2.2.7 the passage throughflow can be calculated using the velocity field for each time step. To do this a suitible location was chosen for each time step and passage such that there are no boundaries next to the passageways. This method is the same for each of the passages, noting that only zonal flow was studied. Thus we can study the effect of changes in bathymetry to on the relative strength of the flow. The passageways have been labeled in figure (figure of these). The computed throughflow can be seen in fig. 15. In this figure the onset of the ACC is clearly visible. Showing that due to the northward movement of Australia and the deepening of the drake passage the total volume transported by the ACC grows dramatically over time. Furthermore it can be seen that the closure of the drake passage causes the flow through the aghulas passage to reverse in direction. Furthermore, the throughflow through the panama passage is shown to slow due to both the onset of the ACC and the closure of the thetys seaway. Finally reversing the direction of flow through the panama passage at 15Ma due to the total closure of the thetys sea. The reversal of the Indonesian throughflow observed by Mulder et al. 2017 is not observed with total throughflow always moving water east to west. This is however in agreement to the flow found by Omta and Dijkstra 2003 in a shallow water model. Note however, that the land masks used by them are different to the land masks used in this paper.

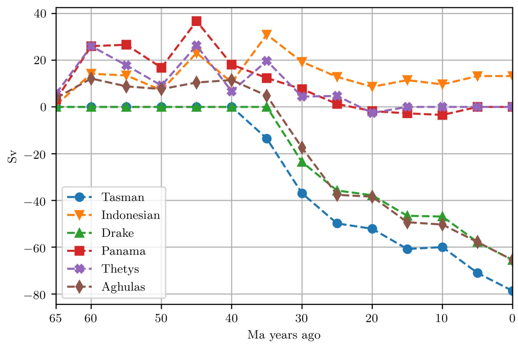

Figure 15: Total volume transport in Sverdups for 7 passages. Running from 65 milion years ago to the present day situation. Positive values indicate transport to the west

Rather than looking only at volume transport in the upper layers the transport can also be split into a deep water transport layer ($< -2000m$) and a surface transport layer($> -2000m$). Doing this gives insight into the thermohaline circulation. In the deep water transport layer seen in fig. 16 we see a very diffirent picture to the total volume transport. It is however hard to draw any conclusions from this image. It is only 6 integration layers deep and fluctuations in the depth of each passage accounts for most of the differences comparing each time step.

To get an even better understanding of the flows, we can look at a vector field showing the direction of horizontal water displacement for each of the time steps. This is done by making a weighted mean of the horizontal flow field for each layer. Weighted by the volume of each grid cell. In this way each arrow actually represents relative flow velocity compared to other grid points. Thus showing the velocity field of the ocean.

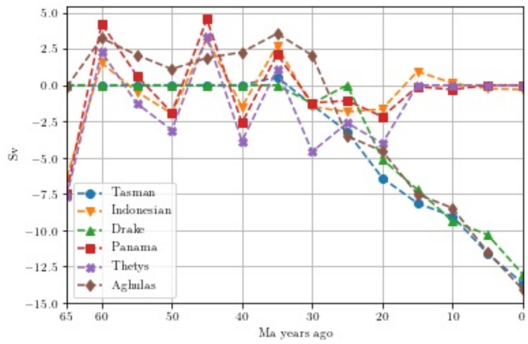

Figure 16: Total volume transport in the deep water layer ($< -2000m$) in Sverdups for 7 passages. Running from 65 milion years ago to the present day situation. Positive values indicate transport to the west

This field is shown in fig. 17. Here the ACC is very noticible. The reversal of flow through the panama passage at $15Ma$ is the most interesting result here. Where here we find the closure of the Thetys seaway to be the main factor. However, the reversal only occurs after the closure of the seaway. This is in contrast to the results obtained by Omta and Dijkstra 2003 where the flow reversal was observed to coincide with the opening of the drake passage. Here we only observe a decease in volume transported through the passage, but no such reversal until the Thetys seaway is closed.

The largest changes in the flow field are observed in the Indian ocean. The indian continent moves northward at a very fast pace. After 55 Ma the flow through the passage north of the Indian continent is massively reduced and instead the water flows east of the continent into the thetys seaway. No "circum India" current is observed in any of the time steps. The position of the Indian continent does however seem to have a strong influence on the strength of the Aghulas sub-tropical gyre. This can probably be explained by the amount of water that is transported through the Tethys seaway. There being a large fluctuation in the strength of the gyre. The size of this gyre also increases with time due to this northward movement.

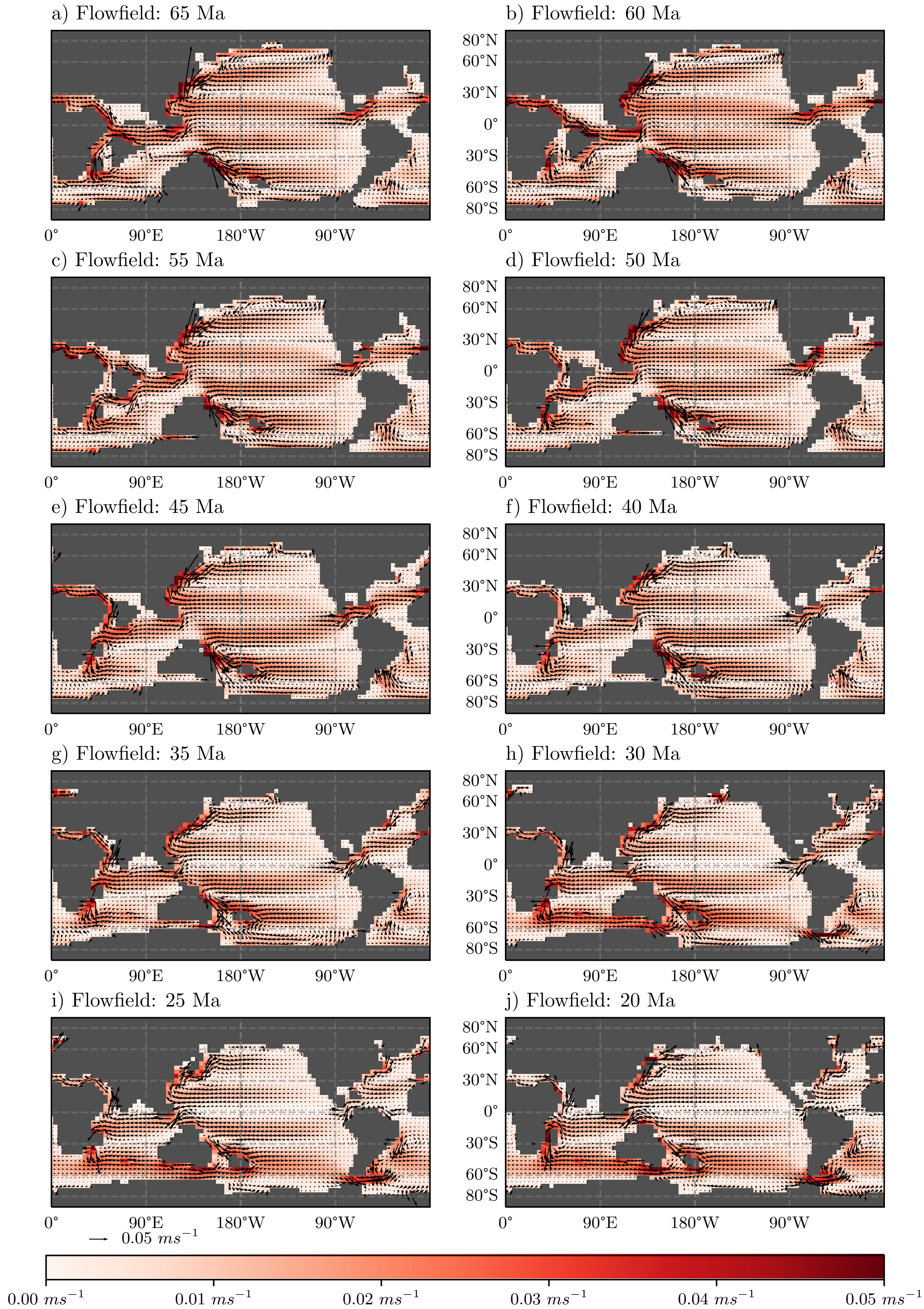
a) Flowfield: 65 Ma
b) Flowfield: 60 Ma
c) Flowfield: 55 Ma
d) Flowfield: 50 Ma
e) Flowfield: 45 Ma
f) Flowfield: 40 Ma
g) Flowfield: 35 Ma
h) Flowfield: 30 Ma
i) Flowfield: 25 Ma
j) Flowfield: 20 Ma
80°N
60°N
30°N
0°
30°S
60°S
80°S
0°
90°E
180°W
90°W
0.05 ms^{-1}
0.00 ms^{-1}
0.01 ms^{-1}
0.02 ms^{-1}
0.03 ms^{-1}
0.04 ms^{-1}
0.05 ms^{-1}

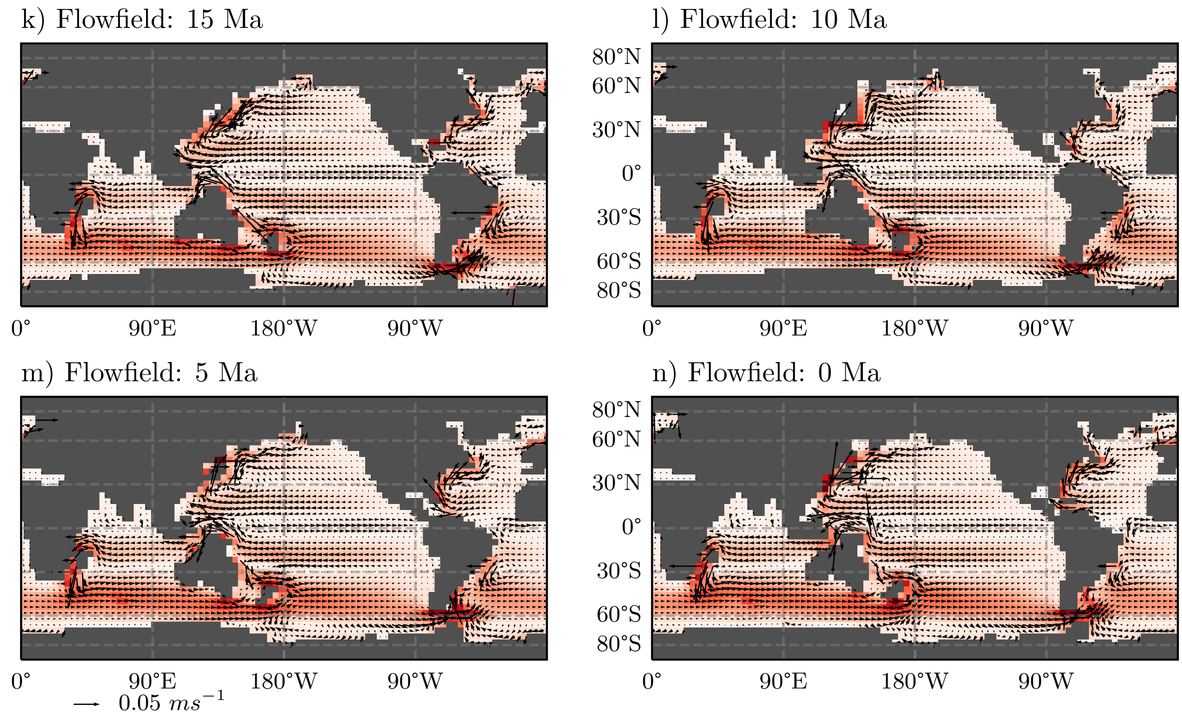

Figure 17: Flow field for each time step, showing the velocity of the vertical column as vectors. The values are in ms^{-1}

3.4 Barotropic Stream function

Next we will look at the barotropic stream function for each of the time steps discussed in this paper. Some of the flows that are discussed in this section are closely related to the flows explained in section 3.3. Here we will have a stronger focus on the gyres seen in the ocean and their relative strength in a time sense. Each of the oceanic basins is discussed in detail. An overview of each of the barotropic stream functions can be seen in fig. 19. The boundary values of the BSF are not shown here. This is due to the previously stated fact that they are excluded from the model output produced by Veros. It must however be noted that this does not mean that flows through the passages are not modeled. In this case the barotropic stream function serves only to see the major ocean gyres and how water is transported in these gyres.

3.4.1 Indian Ocean

The Indian ocean and especially the indian Continent moving northward seems to be one of the most interesting artifacts of these simulations. When the Indian continent is still within the subtropical gyre range in the early Paleocene. We see that it has a large blocking effect on the Subtropical gyre in the Indian ocean. We also see, as observed in the Flow patterns for each of the basins, a change from current moving north over india to moving east and then up towards the Atlantic basin. Something that is simmilarly observed in Omta and Dijkstra 2003. However as noted in section 2.2.7 we do not observe a the often shown circum-India current (Omta and Dijkstra 2003; von der Heydt and Dijkstra 2006). In the Paleocene the Indian continent seems to be the most influential in establishing the ocean gyres. The stark contrast between 65 and 60Ma BSF can be explained due to the island ridge north of India.

3.4.2 Pacific Ocean

The pacific ocean is of particular interest in this case. One of the main things that we see is a large fluctuation in the strength of the southern subtropical gyre. This fluctuation is a diffirence of $\pm 20 Sv$. Especially when the ACC is not yet developed. This is especially visible in the Paleocene and early Eocene where the transport is particularly extreme at places where the Thetys throughflow is the largest. The size of the southern subtropical gyre seems to relate to the Thetys values seen in Figure

15 on page 12. Here we see a round earth current through the Thetys, Indonesian and Panama passages exists. This can explain why such a largely positive streamfunction can be seen in the southern pacific. This Where this only changes with the onset of the ACC.

3.4.3 Atlantic Ocean

The Atlantic basin seems to be the most quiet basin here. This is in large part thanks to the fact that the atlantic basin is so small in the beginning of our time series. One of the flows that is of particular interest here is the subpolar gyre that exists the entire time until the onset of the ACC where it is replaced. The onset of the ACC also seems to coincide with the growth of the southern subtropical gyre. Also the northern subpolar gyre is hardly visible here at all. This is likely due to low resolution used by this model not being able to have proper in and outflow of the arctic sea here.

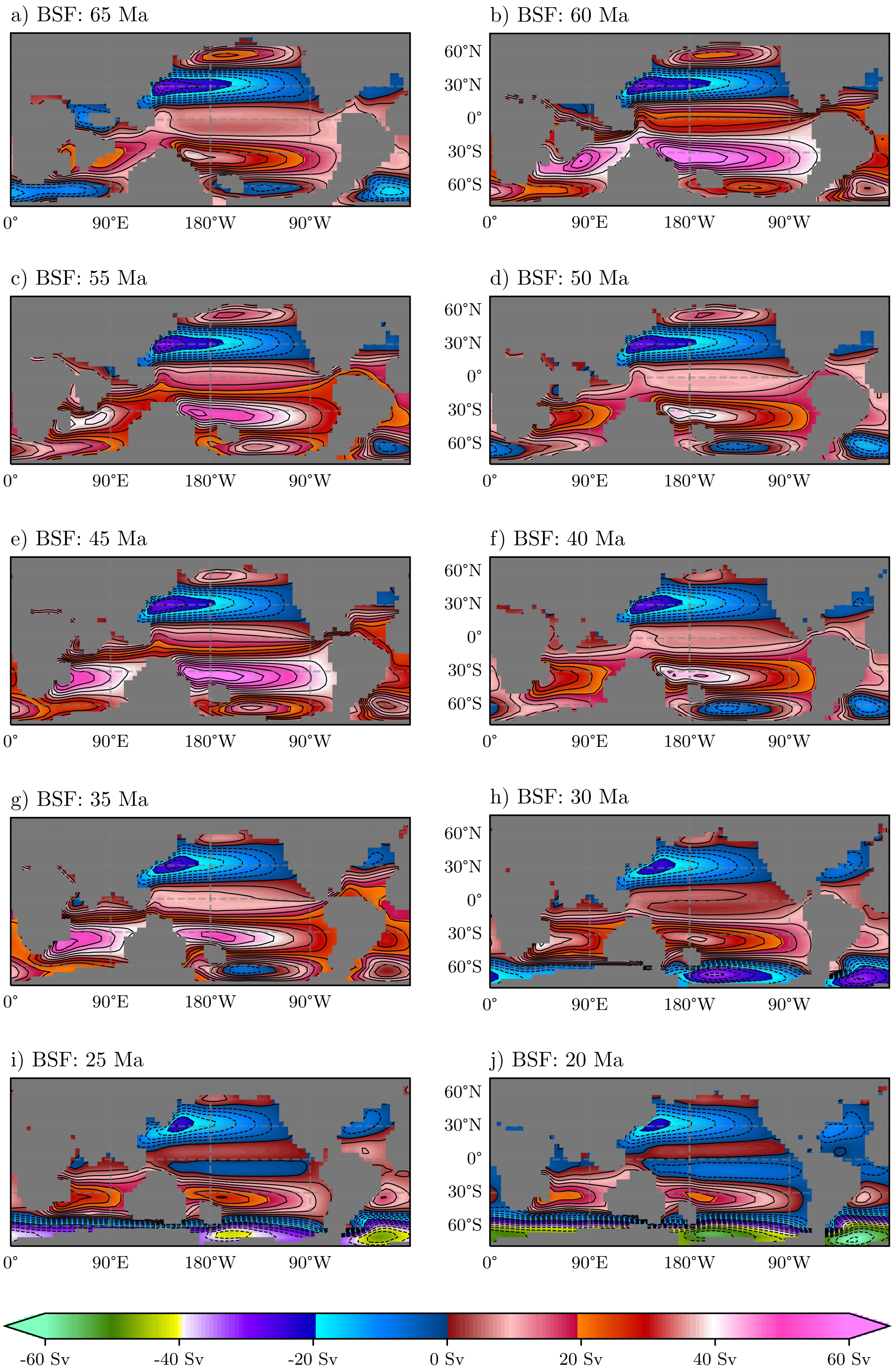
a) BSF: 65 Ma
b) BSF: 60 Ma
c) BSF: 55 Ma
d) BSF: 50 Ma
e) BSF: 45 Ma
f) BSF: 40 Ma
g) BSF: 35 Ma
h) BSF: 30 Ma
i) BSF: 25 Ma
j) BSF: 20 Ma
60°N
30°N
0°
30°S
60°S
0°
90°E
180°W
90°W
-60 Sv
-40 Sv
-20 Sv
0 Sv
20 Sv
40 Sv
60 Sv

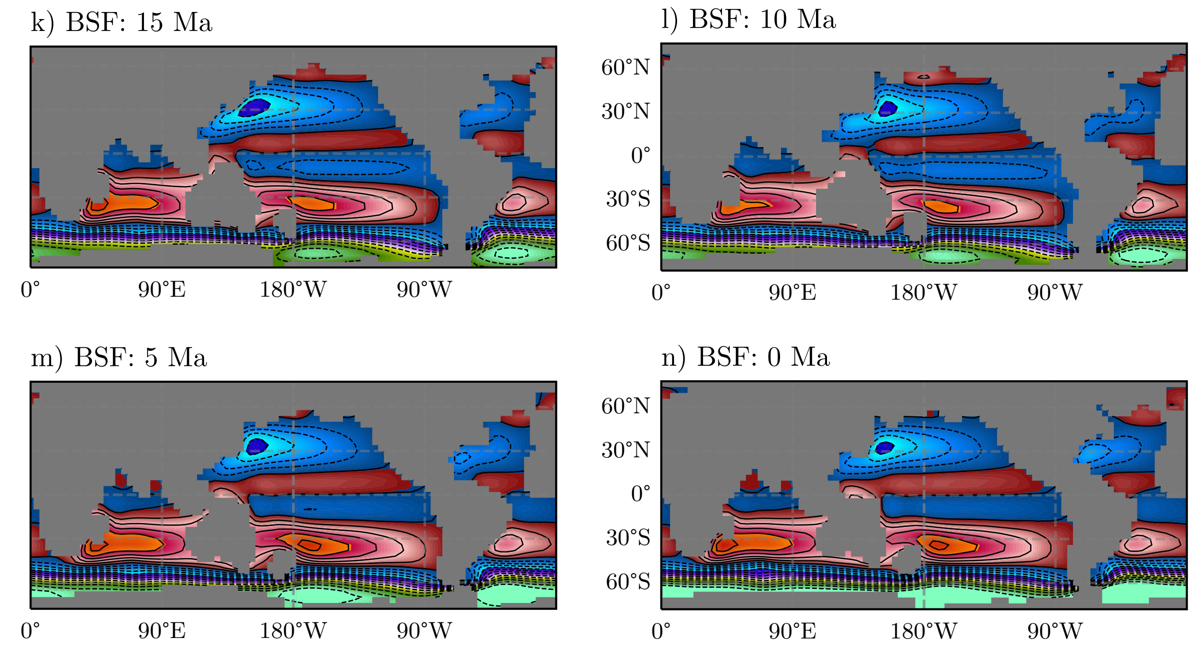

Figure 18: Barotropic Stream Function with contour lines every $5Sv$

3.5 MOC Stream function

Next we will do an analysis on the Global Meridional overturning current stream function (MOC). As mentioned in section 2.2.5 these values will probably not result in a very realistic picture of the overturning circulation. However it still gives us a rough general idea of the deep ocean flows of the thermohaline circulation. This section will again be split into the time periods as defined in section 2.3. The main focus will be on wind driven circulations as they seem to be quite accurately captured as discussed in section 3.2.2.

3.5.1 Paleocene

In the Paleocene one of the most interesting aspect is the southern cell extending from the equator to the antarctic continent. A strong ($9Sv$) southern cell exists. This cell is largely responsible for the mostly positive nature of the overturning circulation seen in the BSF.

(need to research more)

3.5.2 Eocene

In the Eocene we observe little difference to the stream function in the Paleocene. The most interesting feature is the southern subpolar grye. Which starts to extend downwards like the ACC in the present day. The antarctic bottomwater cell is subsequently significantly reduced in strength. The origin of this "ACC-like" cell at 35Ma is attributed to the opening of the Tasman passage in the bathymetry. This is similar to the open Tasman and closed Drake passage case shown by Sijp, England, and Huber 2011.

3.5.3 Oligocene

The Oligocene is characterized by the strong onset of the ACC and a subsequent decrease in size of the south polar cell. It being "pushed" aside due to the strong ACC currents. Another interesting artifact of this is that in the $30Ma$ setup a kind of overturning current is observed. This is however not shown in the 25 and 20 Ma time steps. It should be noted that the deep water cells (¡-2000 m) in all of these are still too weak to be of any realistic value. The Oligocene does seem to harbour some of the strongest Polar cells in any of the models. This was not necicarily observed in the Pictures of the BSF.

3.5.4 Miocene

The Miocene shows some of the main features of the MOC. One of these is the overturning current previously mentioned. It is however important to note that it is still really weak compared to other models with more depth layers and observations (von der Heydt and Dijkstra 2006). Probably due to the fact that the overturning circulation in the Atlantic is absent in this model. This may simply be a case of boundary conditions but could also be explained by the relatively weak SSS forcings in the Atlantic compared to real world values. In the last 15 Ma we see very little change overall in the MOC stream function. We see mostly fluctuations in the northern sub polar cell.

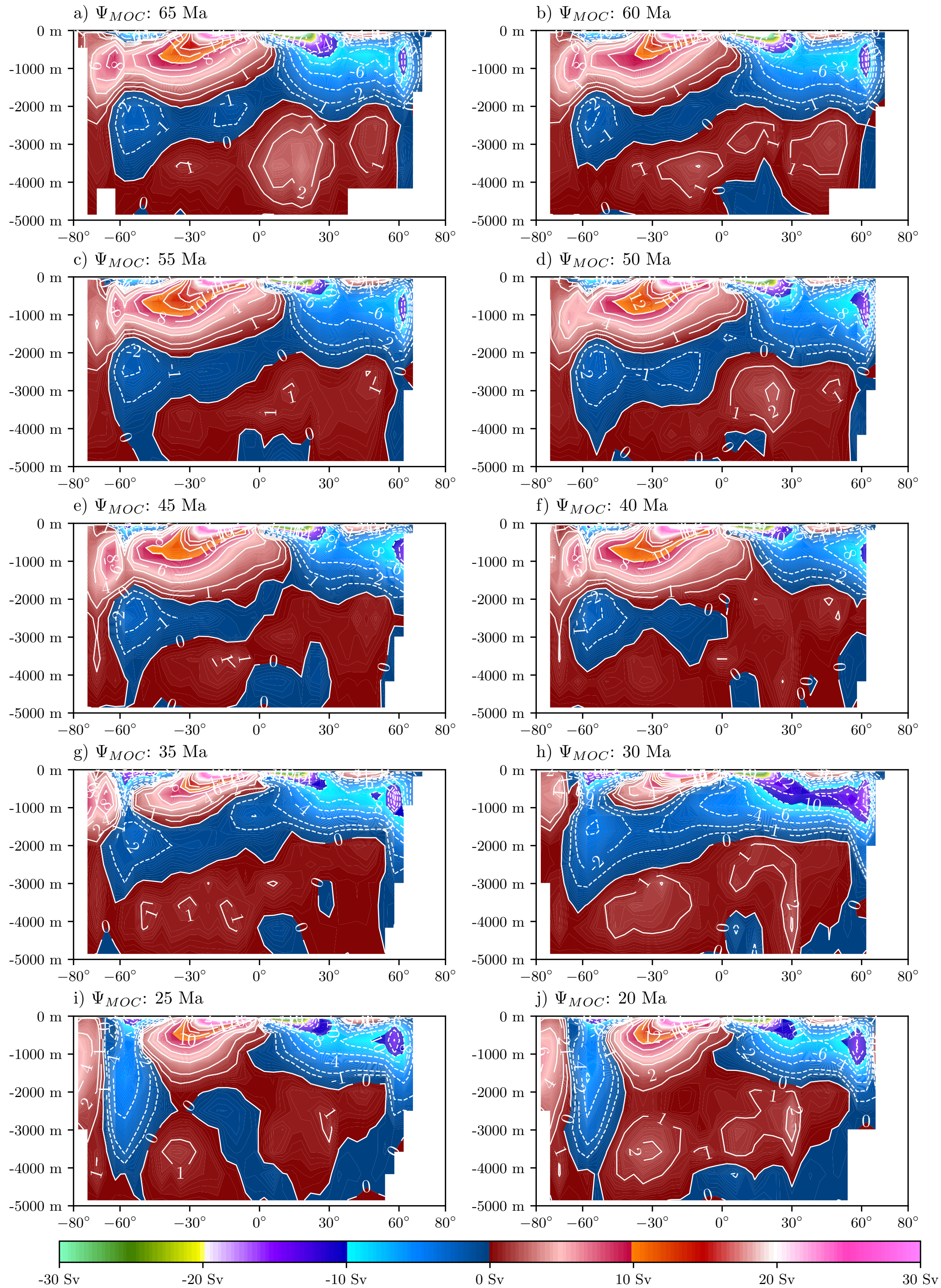
a) Ψ_{MOC}: 65 Ma
b) Ψ_{MOC}: 60 Ma
c) Ψ_{MOC}: 55 Ma
d) Ψ_{MOC}: 50 Ma
e) Ψ_{MOC}: 45 Ma
f) Ψ_{MOC}: 40 Ma
g) Ψ_{MOC}: 35 Ma
h) Ψ_{MOC}: 30 Ma
i) Ψ_{MOC}: 25 Ma
j) Ψ_{MOC}: 20 Ma
0 m
-1000 m
-2000 m
-3000 m
-4000 m
-5000 m
−80°
−60°
−30°
0°
30°
60°
80°
-30 Sv
-20 Sv
-10 Sv
0 Sv
10 Sv
20 Sv
30 Sv

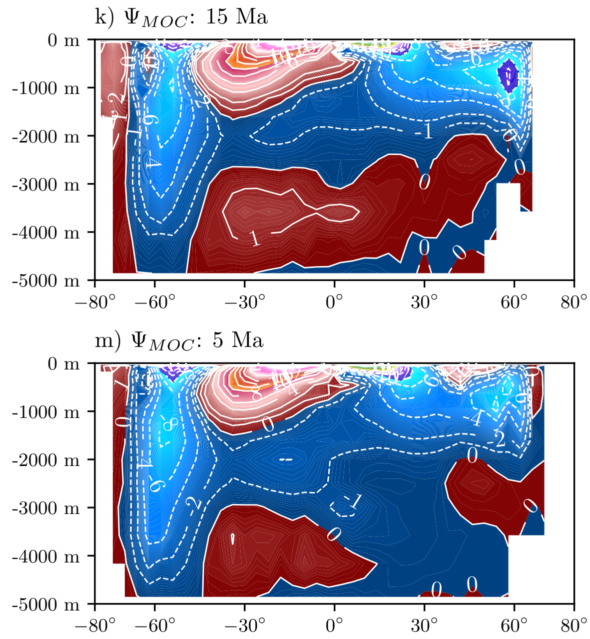

Figure 19: Barotropic Stream Function

4 Global Thermohaline circulation

I have started reading up some more on the subject of the Thermohaline circulation but i have gotten stuck with this part. The figures in this part of the paper seem to indicate quite dramatic diffirences between the diffirent setups. But i find it hard to make solid arguments supporting a conclusion on the shape of the thermohaline circulation. I would have liked to have been able to make a heat transport figure. These I often came across in my research, I have however been unable to find how to make this in Veros.

To get a better picture of the changes that occur during the time periods we compare differences in sea temperature at 250m depth. We do not use the sea surface temperature here because of the restoring boundary conditions used on the top layer of the ocean. Thus we can get a better idea of the transported temperature. First, we compare the temperature diffirence in the 55Ma basin and the 35Ma basin. We thus compare the temperature profiles of the late Paleocene to the late Eocene (Figure 20 on page 20). Here we see substantial diffirences between the two. One of the key features of the Eocene seems to be a large amount of cooling in the southern Atlantic along with a heating in the southern pacific. Resulting from the large Increase in size of the southern subtropical gyre in the Indian ocean.

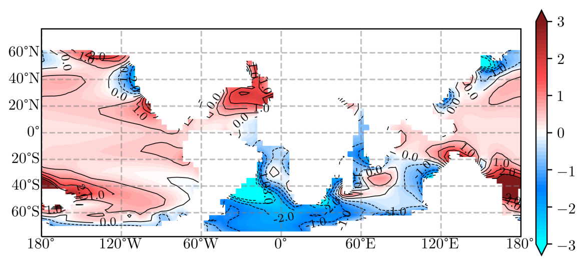

Figure 20: Temperature $°C$ diffirences between late Paleocene (55Ma) and late Eocene (35Ma) simulations. Positive values indicate warming, Negative values indicate cooling.

We also look at the changes between the late Eocene and the late Oligocene.

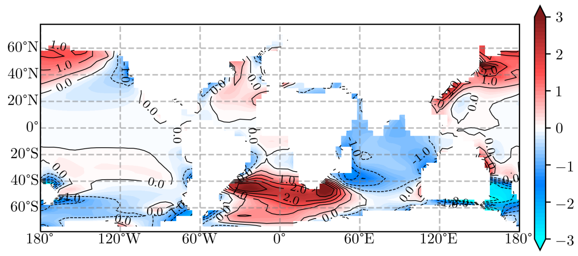

Figure 21: Temperature °C diffirences between late Eocene (35Ma) and late Oligocene (20Ma) simulations. Positive values indicate warming, Negative values indicate cooling.

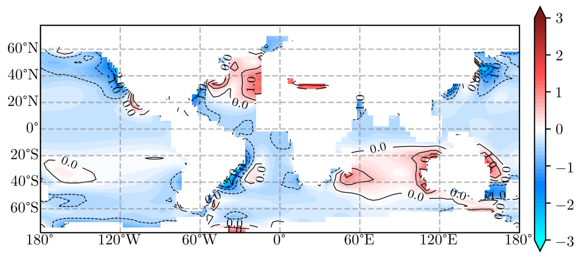

Figure 22: Temperature diffirences °C between late Oligocene (20Ma) and middle Miocene (10Ma) simulations. Positive values indicate warming, Negative values indicate cooling.

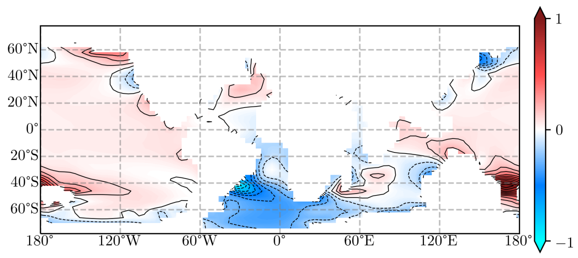

Figure 23: Salinity (psu) differences between late Paleocene (55Ma) and late Eocene (35Ma) simulations at 245m depth. Positive values indicate warming, Negative values indicate cooling.

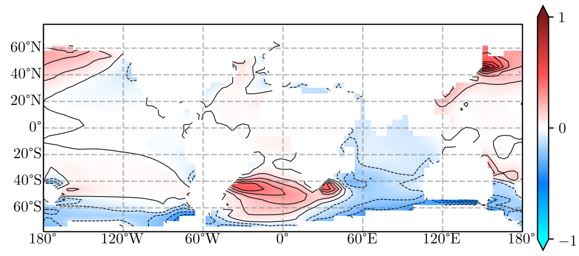

Figure 24: Salinity (psu) differences between late Eocene (35Ma) and late Oligocene (20Ma) simulations at 245m depth. Positive values indicate warming, Negative values indicate cooling.

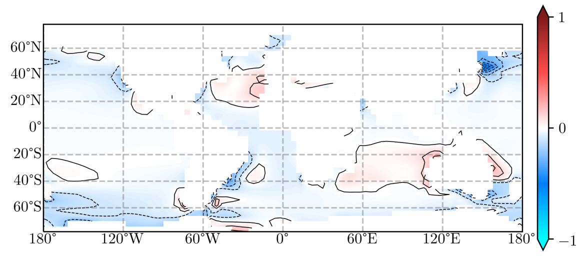

Figure 25: Salinity (psu) differences between late Oligocene (20Ma) and middle Miocene (10Ma) simulations at 245m depth. Positive values indicate warming, Negative values indicate cooling.

5 Summary

In this paper we have presented a simplified approach to the modeling of past climate systems using Veros. This paper focused heavily on simplified forcings of the global oceanic basins. This allows us to efficiently look at the effect of changes in geometry on the major oceanic flows. The results shown here are of relatively low resolution and highly idealized boundary conditions. But they still manage to capture some of the features of more complex coupled models for the same time period. The integrations were done on a consumer computer showing that it is possible to do even larger ocean simulation research on readily available hardware.

In the barotropic stream functions we observed high variability between the different integrations. Especially in the Paleocene where it was mainly attributed to the large variation in the Indian ocean. It thus appears that the exact location of the Indian continent may have had profound implications on the past oceanic circulations. In our study of the passage throughflow we find that there is a flow reversal in the panama passage after the closure of the thetys seaway. Here we also find large variability in the passage throughflows before the onset of the Antarctic circumpolar current. Furthermore, we observe flow reversal in the Aghulas passage occurring simultaneously to the opening of the drake passage.

We were unable to accurately predict the meridional overturning circulation. We do find some evidence for a total absence of transport over the equator before the onset of the ACC.

In general we observe a wind driven circulation that quite accurately manages to capture the volume transport in the upper layers of the ocean. We find that using zonally averaged forcings does have major implications on the strength of the flows due to large zonal changes in all of the forcings. We can conclude that the simulations were quite succesful in capturing an overall image of the wind driven circulation but require much higher resolution to be useful in research. This is however a change that is quite easily made using Veros.

I still wish to add something in the conclusion: On the inaccuracy of the bathymetries Significance of India in the wind driven circulation.

6 Discussion

The method presented here for an alternative to the continuation approach suggested by Mulder et al. 2017 still has quite a few problems. First of all the 4° resolution together with the limited number of depth layers is one of the main problems. The limited depth layers fail to accuratly capture even the present day overturning circulation. Here we note that the same can be said for a model with present day forcings as noted in section 3.2.2. Next, we also note that an ACC strength of just $80Sv$ is a lot lower than the observed 100-150 Sv. This can mainly be attributed to the weaker wind forcings in the southern hemisphere. The present day zonal wind forcing being more than 50% stronger.

The possibility of using a 1 or 2 degree Veros model for this paper was extensively explored. But issues often arose with the exact values of constants and frequent invalid value errors to do with eddy kinetic energy could not be fixed in time for this paper.

The 4 degree model also took quite a bit of time to be adapted for the customized forcings and bathymetries. This is due to the fact that the method for determining boundary conditions for islands would often find more islands than exist in the model. Resulting in having to customize each setup individually for its bathymetry to accept the islands present. This is also why $180°E$ was used as the boundary longitude instead of the default 0°.

Another major thing that is generally neglegted in this paper is the total absence of change in surface forcings. Even though it is known that these change drastically even in short time spans. We also have some general knowledge of global average temperature for the time period discussed here. However the search for a dataset for each time step has proven futile. Often large uncertainties exist. This left us with the decision to not bother with any changes in the forcings. Even though there have been massive changes in the time period discussed here. Coupled with the sensitive nature of GCM's we suggest taking the results in this paper with a grain of salt.

A lot of future research is possible in the topic of oceanic throughflow. More accurate bathymetries are being produced due to breakthroughs in geological techniques (Baatsen et al. 2016). These, coupled with a higher resolution model will probably result in even more accurate depictions of the past oceanic systems. Research on this topic is of particular importance because of the present day observed changes in strength of the MOC.

7 Acknowledgments

This paper would not have been possible without the extensive support of Dr. Anna von der Heydt, who provided valuable input on every single one of the many hurdles that had to be succumbed. I would also like to thank Dr. Michiel Baatsen for providing the bathymetry datasets used in this paper, Prof. Dr. Markus Jochum for providing valuable insight into Veros and Laurits Andreasen for helping with many of our questions and attending our virtual meetings.

References

[1] Jean Besse and Vincent Courtillot. "Apparent and true polar wander and the geometry of the geomagnetic field over the last 200 Myr". In: *Journal of Geophysical Research: Solid Earth* 107.B11 (2002), EPM–6.

[2] Howie D. Scher and Ellen E. Martin. “Timing and Climatic Consequences of the Opening of Drake Passage”. In: *Science* 312.5772 (2006), pp. 428–430. ISSN: 0036-8075. DOI: 10.1126/science.1120044.

[3] D. N. Schmidt. “The closure history of the Panama Isthmus: Evidence from isotopes and fossils to models and molecules”. In: *ResearchGate* (2007), p. 429444. URL: https://www.researchgate.net/publication/282323290_The_closure_history_of_the_Panama_Isthmus_Evidence_from_isotopes_and_fossils_to_models_and_molecules.

[4] Wallace S Broecker. “The great ocean conveyor”. In: *Oceanography* 4.2 (1991), pp. 79–89.

[5] Meir Abelson and Jonathan Erez. “The onset of modern-like Atlantic meridional overturning circulation at the Eocene-Oligocene transition: Evidence, causes, and possible implications for global cooling”. In: *Geochemistry Geophysics Geosystems* 18 (May 2017). DOI: 10.1002/2017GC006826.

[6] T. E. Mulder et al. “Efficient computation of past global ocean circulation patterns using continuation in paleobathymetry”. In: *Ocean Modell.* 115 (2017), pp. 77–85. ISSN: 1463-5003. DOI: 10.1016/j.ocemod.2017.05.010.

[7] Dion Hafner et al. “Veros v0.1 - a fast and versatile ocean simulator in pure Python”. In: *Geosci. Model Dev.* 11.8 (2018), p. 3299. ISSN: 1991-959X. URL: https://go.gale.com/ps/anonymous?id=GALE%7CA550451036&sid=googleScholar&v=2.1&it=r&linkaccess=abs&issn=1991959X&p=AONE&sw=w.

[8] Ralph F. Milliff et al. “Ocean general circulation model sensitivity to forcing from scatterometer winds”. In: *J. Geophys. Res. Oceans* 104.C5 (1999), pp. 11337–11358. ISSN: 0148-0227. DOI: 10.1029/1998JC900045.

[9] Frank Bryan. “Parameter sensitivity of primitive equation ocean general circulation models”. In: *Journal of Physical Oceanography* 17.7 (1987), pp. 970–985.

[10] Andreas Schmittner and Thomas F Stocker. “A seasonally forced ocean–atmosphere model for paleoclimate studies”. In: *Journal of climate* 14.6 (2001), pp. 1055–1068.

[11] ECMWF. *ECMWF | CAMS Climate Forcing Estimates*. 2020.

[12] James Hansen et al. “Climate sensitivity, sea level and atmospheric carbon dioxide”. In: *Philosophical transactions. Series A, Mathematical, physical, and engineering sciences* 371.2001 (2013). DOI: 10.1098/rsta.2012.0294.

[13] G. Forget et al. “ECCO version 4: an integrated framework for non-linear inverse modeling and global ocean state estimation”. In: *Geosci. Model Dev.* 8.10 (2015), pp. 3071–3104. ISSN: 1991-959X. DOI: 10.5194/gmd-8-3071-2015.

[14] Harald Ulrich Sverdrup. “Wind-driven currents in a baroclinic ocean; with application to the equatorial currents of the eastern Pacific”. In: *Proceedings of the National Academy of Sciences of the United States of America* 33.11 (1947), p. 318.

[15] R. Alan Plumb John Marshall. “Atmosphere, Ocean and Climate Dynamics: An Introductory Text”. In: San Diego, California: Elsevier Acedemic Press, 2012. Chap. The wind-driven circulation, p. 214. ISBN: 978-0125586917.

[16] Michiel Baatsen et al. “Reconstructing geographical boundary conditions for palaeoclimate modelling during the Cenozoic”. In: *Clim. Past* 12.8 (2016), pp. 1635–1644. ISSN: 1814-9324. DOI: 10.5194/cp-12-1635-2016.

[17] Roy Livermore et al. “Paleogene opening of Drake Passage”. In: *Earth Planet. Sci. Lett.* 236.1 (2005), pp. 459–470. ISSN: 0012-821X. DOI: 10.1016/j.epsl.2005.03.027.

[18] O. Jagoutz, P. Bouilhol, and Rajeev Upadhyay. “Geology of the Kohistan-Ladakh arc and its relation to the main Himalayan belt”. In: *AGU Fall Meeting Abstracts* (Dec. 2009).

[19] Lawrence A. Lawver and Lisa M. Gahagan. “Evolution of Cenozoic seaways in the circum-Antarctic region”. In: *Palaeogeogr. Palaeoclimatol. Palaeoecol.* 198.1 (2003), pp. 11–37. ISSN: 0031-0182. DOI: 10.1016/S0031-0182(03)00392-4.

[20] Sudipta Sarkar et al. “Late Eocene onset of the Proto-Antarctic Circumpolar Current”. In: *Sci. Rep.* 9.10125 (2019), pp. 1–10. ISSN: 2045-2322. DOI: 10.1038/s41598-019-46253-1.

[21] Yani Najman et al. "Timing of India-Asia collision: Geological, biostratigraphic, and palaeomagnetic constraints". In: *J. Geophys. Res. Solid Earth* 115.B12 (2010). ISSN: 0148-0227. DOI: 10.1029/2010JB007673.

[22] N. Hamon et al. "The role of eastern Tethys seaway closure in the Middle Miocene Climatic Transition (ca. 14 Ma)". In: *Clim. Past* 9.6 (2013), pp. 2687–2702. ISSN: 1814-9332. DOI: 10.5194/cp-9-2687-2013.

[23] Peter Molnar. "Closing of the Central American Seaway and the Ice Age: A critical review". In: *Paleoceanography* 23.2 (2008). ISSN: 0883-8305. DOI: 10 . 1029 / 2007PA001574.

[24] James L. Pindell et al. "A plate-kinematic framework for models of Caribbean evolution". In: *Tectonophysics* 155.1 (1988), pp. 121–138. ISSN: 0040-1951. DOI: 10.1016/0040-1951(88)90262-4.

[25] Anna von der Heydt and Henk A Dijkstra. "Effect of ocean gateways on the global ocean circulation in the late Oligocene and early Miocene". In: *Paleoceanography* 21.1 (2006).

[26] Anne Willem Omta and Henk A Dijkstra. "A physical mechanism for the Atlantic–Pacific flow reversal in the early Miocene". In: *Global and planetary Change* 36.4 (2003), pp. 265–276.

[27] Peter H Stone and James S Risbey. "On the limitations of general circulation climate models". In: *Geophysical Research Letters* 17.12 (1990), pp. 2173–2176.

[28] James Hansen et al. "Ice melt, sea level rise and superstorms: evidence from paleoclimate data, climate modeling, and modern observations that 2 degree global warming could be dangerous". In: *Atmos. Chem. Phys.* 16.6 (2016), pp. 3761–3812. ISSN: 1680-7316. DOI: 10.5194/acp-16-3761-2016.

[29] Willem P. Sijp, Matthew H. England, and Matthew Huber. "Effect of the deepening of the Tasman Gateway on the global ocean". In: *Paleoceanography* 26.4 (2011). ISSN: 0883-8305. DOI: 10.1029/2011PA002143.

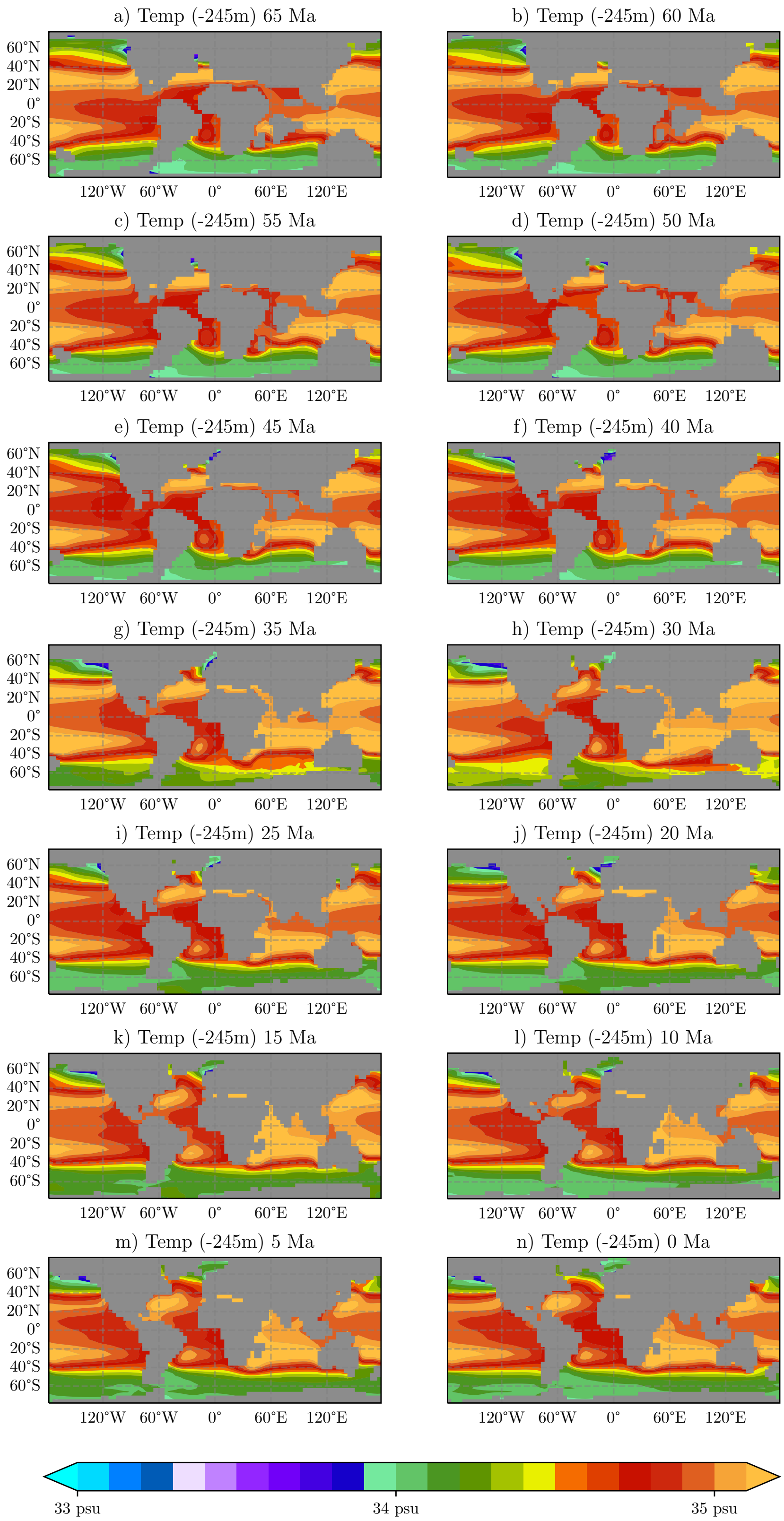

Figure 26: Salinity at 245m depth for each time step.

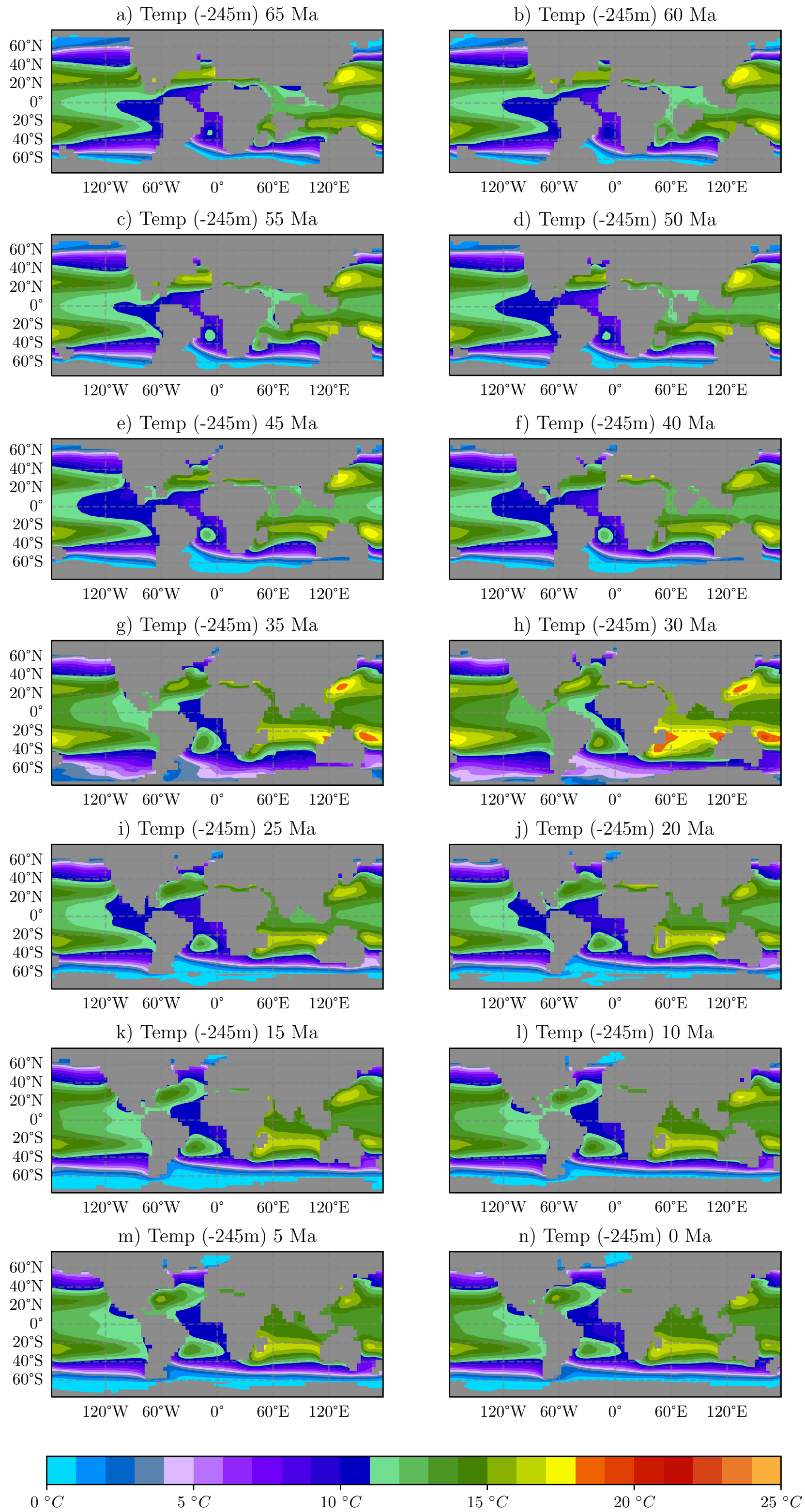

Figure 27: Temperature at 245m depth for each time step.

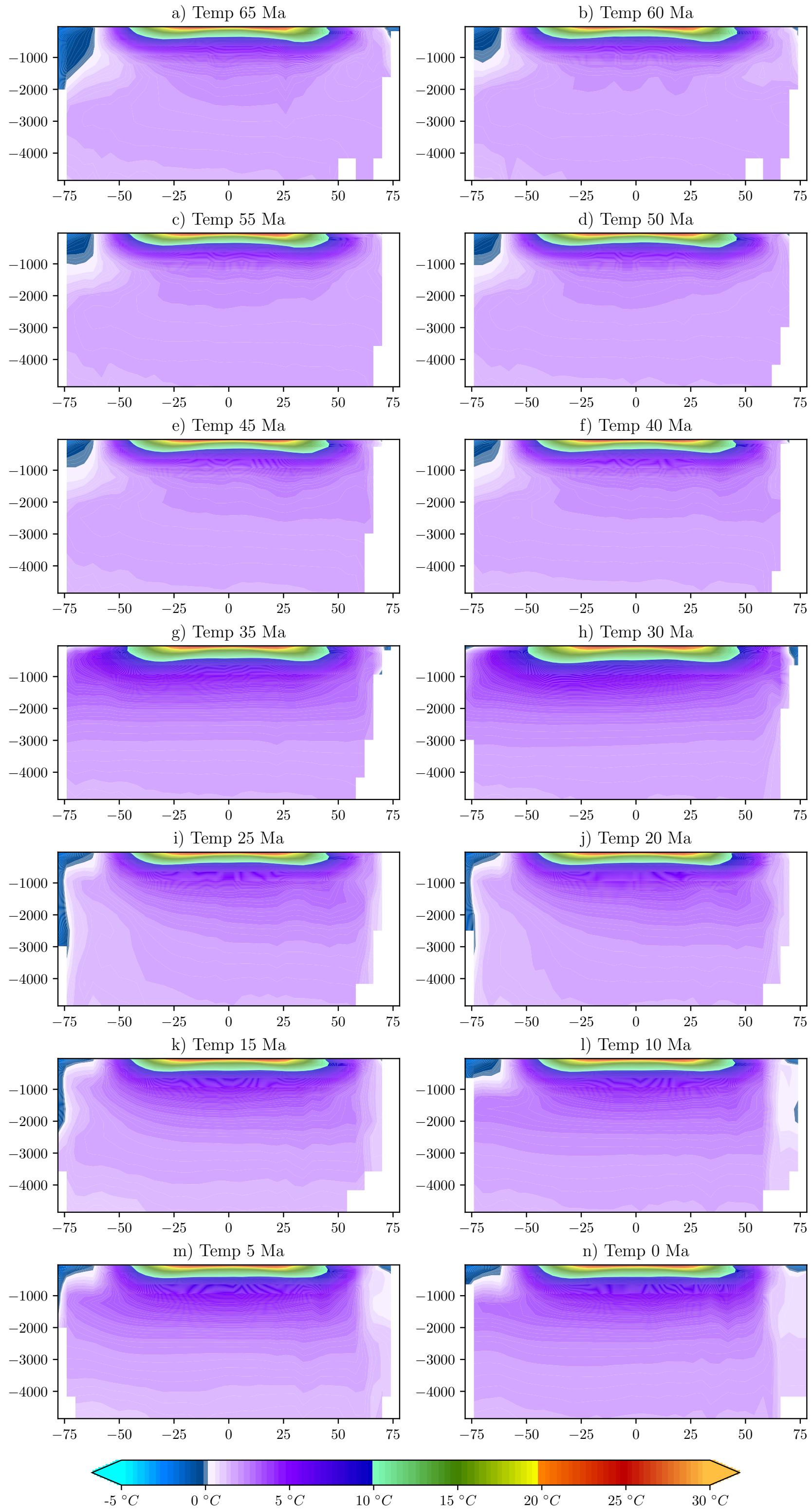

Figure 28: Latitude depth profile of the zonal mean Temperature

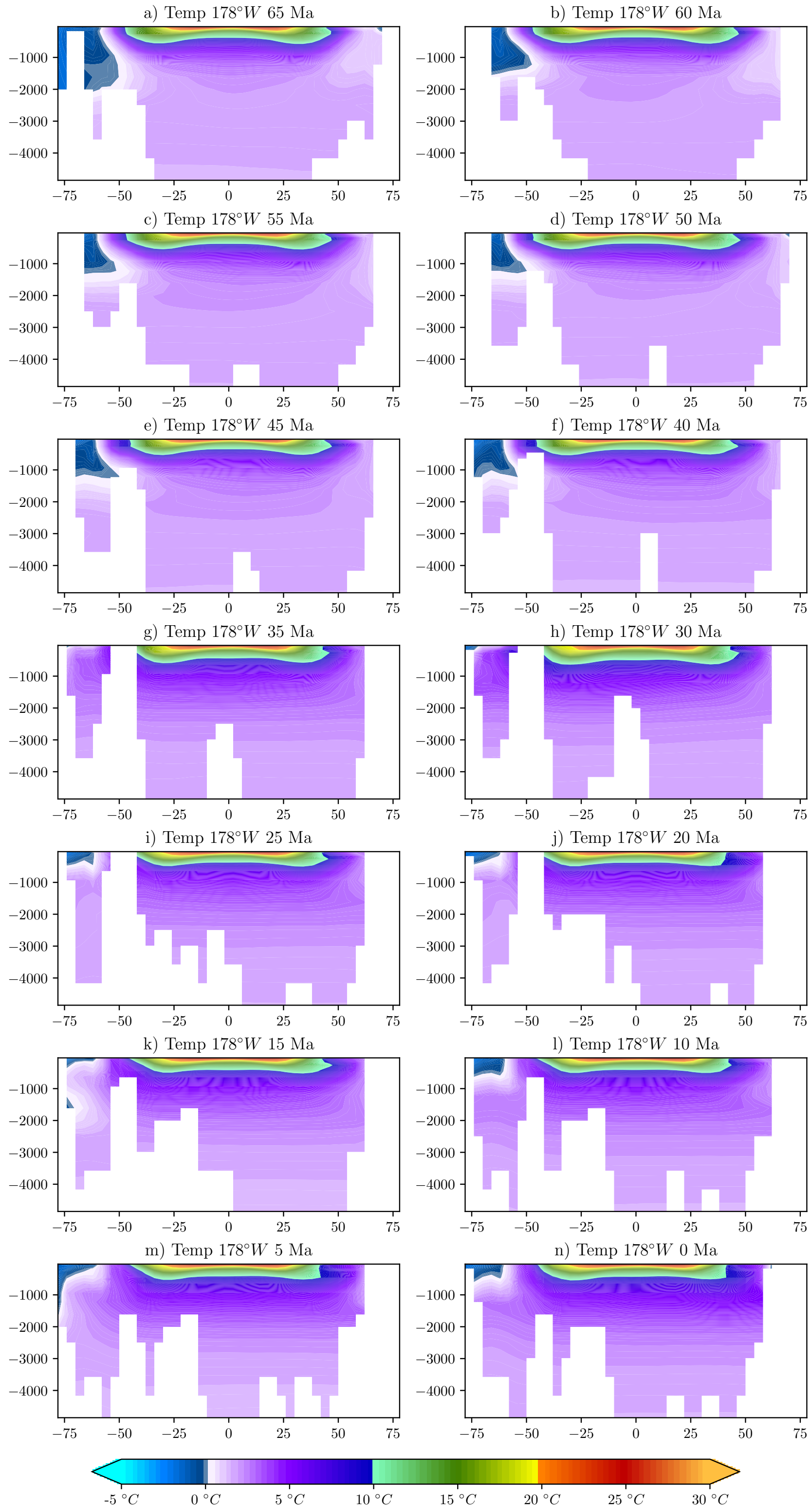

Figure 29: Latitude depth profile of the Temperature in the Pacific ($178°W$)

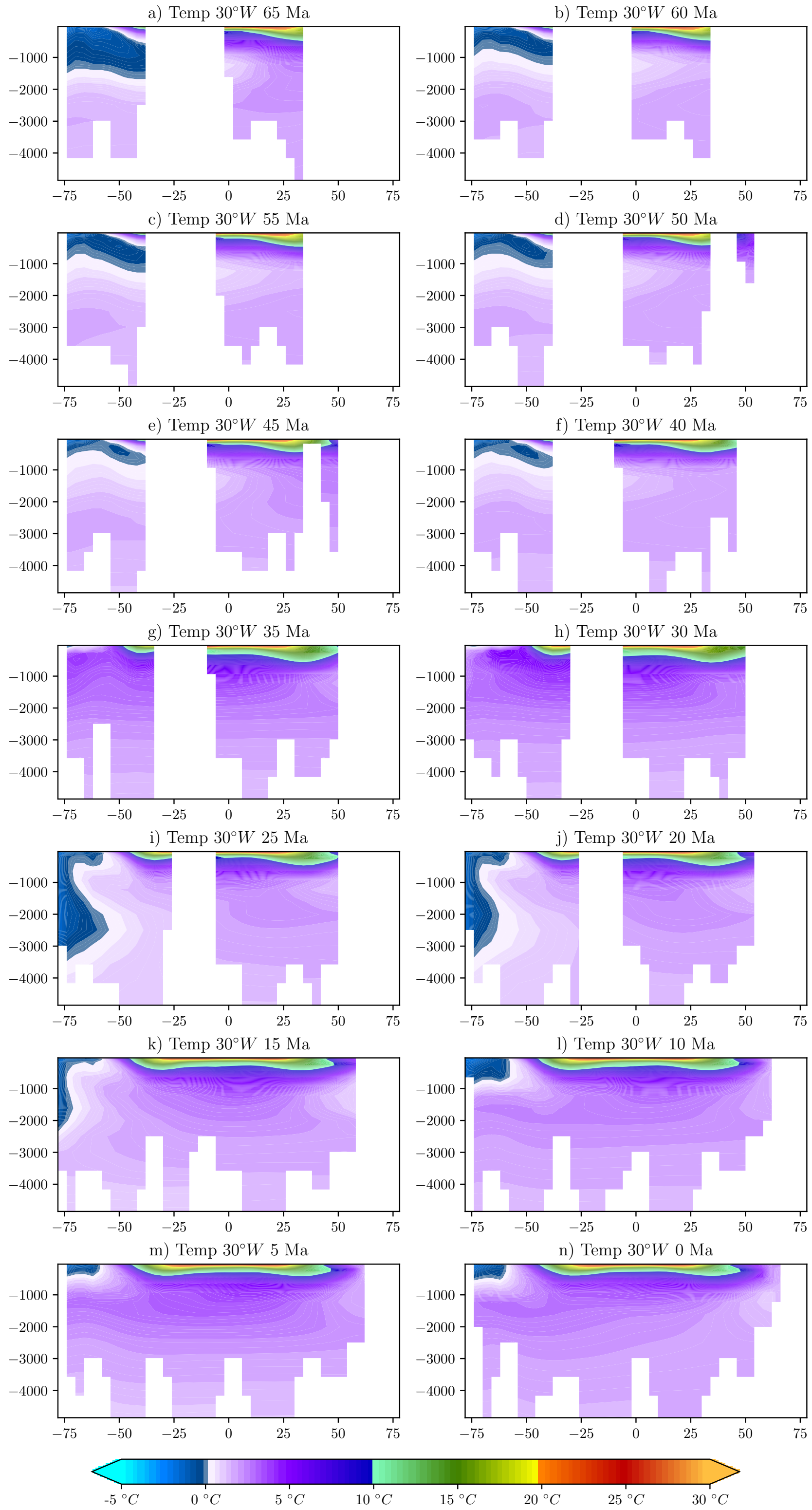

Figure 30: Latitude depth profile of the Temperature in the Atlantic (178°W)

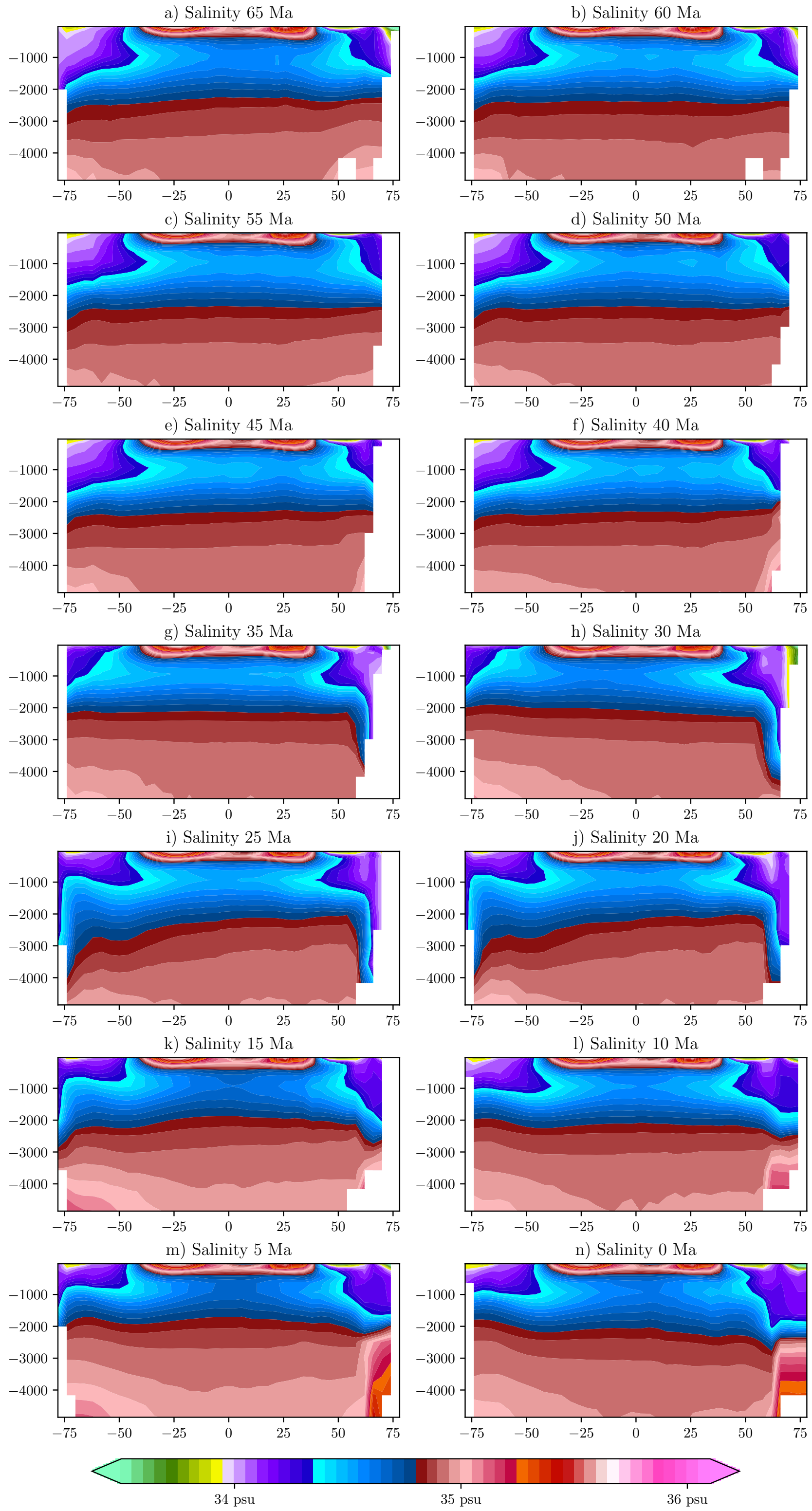

Figure 31: Latitude depth profile of the zonal mean Salinity